Supplementary Information (SI) for Chemical Science.
This journal is © The Royal Society of Chemistry 2026

Supporting Information for

Tetraphenylborate-Based Anionic Metal−Organic Framework as an Efficient Single-Ion Conductor for Solid-State Sodium Battery

Xiaoxin Liu,[1]† Zhiwei Lu,[1]† Qianyi Zhao,[1,]* Shujun Li,[1,]* Jie Zhang,[1] Xuenian Chen,[1,2] and Qingchun Xia[1,]*

[1]*Henan Key Laboratory of Boron Chemistry and Advanced Materials, School of Chemistry and Chemical Engineering, Henan Normal University, Xinxiang, Henan 453007, China.*

[2]*College of Chemistry, Zhengzhou University, Zhengzhou, Henan 450001, China.*

† X.L. and Z.L. contributed equally to this work

*Email: qyzhao@htu.edu.cn; lisj@htu.edu.cn; xiaqingchun@htu.edu.cn

Table of Content

1 Materials and general procedures

All reagents and solvents used in these studies are commercially available and used without further purification. The IR (KBr pellet) spectra were recorded (400-4000 cm^{-1} region) on a Nicolet Magna 750 FT-IR spectrometer. Thermogravimetric analyses (TGA) were carried out in an air atmosphere with a heating rate of 10 ^oC/min on a STA449C integration thermal analyzer. Powder X-ray diffraction (PXRD) data were collected on D8 advance diffractometer with Cu Kα radiation of wavelength (λ) = 1.5418 Å at 40 kV and 40 mA in the reflection mode. The step size was 0.02° with an exposure time of 5 s per step. The calculated PXRD patterns were produced using the SHELXTL-XPOW program and single-crystal reflection data. The NMR experiments were carried out on a MERCURYplus 400 spectrometer operating at resonance frequencies of 400 MHz. Transmission electron microscopy (TEM) images were obtained on a Talos F200X/TALOS F200X instrument. Atomic force microscope (AFM) images were obtained on an Environment Control Scanning Probe Microscope (Nanonavi E-Sweep). The samples for AFM measurements were prepared by placing a drop of the diluted nanosheet dispersion onto a fresh cleaved mica. Scanning Electron Microscopy (SEM) images were performed on a NOVA NanoSEM 230 instrument equipped with an energy dispersive spectroscopy (EDS) detector. X-ray photoelectron spectroscopy (XPS) was recorded on a AXIS Ultra DLD surface analysis instrument. The CO_2 adsorption isotherms were recorded at 273K by using a micromeritics ASAP 2020 surface area and porosity analyzer. Before the adsorption measurement, the samples were activated at 80 ^oC under vacuum (< 10^{-3} torr) for 4 h. The UV spectra were recorded in the range of 260-800 nm at room temperature with a UV/Vis Spectrometer Lambda 35 (Perkin Elmer, Inc., USA).

Single-crystal XRD data for **1** were collected on a Bruker SMART Apex II CCD-based X-ray diffractometer with Cu-Kα radiation (λ = 1.54178 Å) at 150 K. The empirical absorption correction was applied by using the SADABS program (G. M. Sheldrick, SADABS, program for empirical absorption correction of area detector data; University of Göttingen, Göttingen, Germany, 1996). The structure was solved by direct methods with SHELXS-2018 and refined with SHELXL-2018 using OLEX 1.2. In the structure, all the non-hydrogen atoms were refined by full-matrix least-squares techniques with anisotropic displacement parameters, and the hydrogen atoms were geometrically fixed at the calculated positions attached to their parent atoms, treated as riding atoms. Contributions to scattering due to these highly disordered solvent molecules were removed using the *SQUEEZE* routine of *PLATON*; structures were then refined again using the data generated.

The structure was then refined again using the data generated. Crystal data and details of the data collection are given in **Table S1**. CCDC 2542313 contain the supplementary crystallographic data for this paper. These data can be obtained free of charge from the Cambridge Crystallographic Data Centre via www.ccdc.cam.ac.uk/data request/cif

2 Experimental procedure for synthesis and analysis

2.1 Synthesis of the ligand $Na^+B(PhCOOH)_4^-$

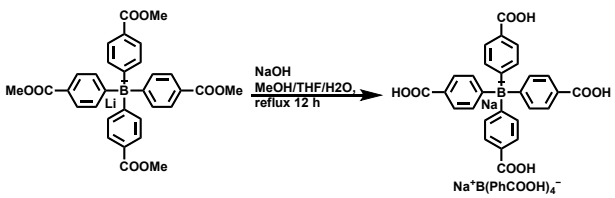

To a mixture of MeOH (40 mL), THF (40 mL) and water (40 mL) in a round-bottom flask, lithium tetrakis (4-(methoxycarbonyl) phenyl) borate (4.1 g, 7.14 mmol), NaOH (1.40 g, 34.08 mmol) were

added. The mixture was refluxed for 16 h. MeOH and THF were removed by evaporation, and the residue was diluted with H_2O and washed with EA for 3 times. The aqueous phase was acidified with concentrated HCl, and the precipitate was collected by filtration and then dried under vacuum to afford 2.32 g of brown solid [$Na^+B(PhCOOH)_4^-$] with 65% yield. ^{1}H NMR (600 MHz, DMSO-d_6): δ = 7.59 (d, J = 8.1 Hz, 8H), 7.25 (m, 8H). ^{11}B NMR (193 MHz, DMSO-d_6): δ = −6.43. ^{13}C NMR (151 MHz, DMSO-d_6):169.37 (m), 168.68, 135.19, 127.09, 125.21.

2.2 Synthesis of 2^{Na}

A mixture of $ZrCl_4$ (116 mg, 0.5 mmol), $Na^+B(PhCOOH)_4^-$ (259 mg, 0.5 mmol), DMF (60 mL), HAc (10 mL) was sealed in a 100 mL vial with a screw cap and heated at 120 °C for 24 h. After that, the colorless crystals were collected, washed with MeOH, and dried under vacuum at 80 °C to afford the **2^{Na}** (305 mg, 68%). The product can be best formulated as $Na_2 \cdot \{Zr_6O_4(OH)_7(H_2O)(CH_3COO)[B(PhCOO)_4]_2\}$ based on single-crystal analysis.

ICP measurement indicated the molar ratio of Na:B:Zr is about 0.88:1:3.11.

IR (KBr, cm^{-1}): 1655 (w), 1590 (w), 1503 (w), 1403 (s), 1283 (w), 1242 (w), 1177 (m), 1032 (m), 763 (m), 721 (w), 638 (s), 576 (w), 508 (w), 456 (s).

2.3 Synthesis of 2^{K}

To a Schlenk tube, 60 mg of **2^{Na}** and 2 mL PC saturated solution of KI were added. The Schlenk tube was then immersed in the oil bath and incubated at 80 °C for 4 h. Subsequently, the crystals were collected via vacuum filtration, and the aforementioned ion exchange experiment was repeated every 4 hours for a total of 5 cycles until no free Na^+ was detected by ICP-MS. The final product was collected, washed with water, and dried under vacuum at 120 °C to afford **2^{K}** as a white free-flowing powder.

ICP measurement indicated the molar ratio of K:B:Zr is about 1.12:1:3.25.

IR (KBr, cm^{-1}): 1652 (m), 1587 (w), 1503 (w), 1403 (s), 1274 (w), 1242 (w), 1108(w), 1045 (w), 763 (m), 718 (w), 644 (s), 576 (m), 514 (m), 456 (s).

2.4 Synthesis of 2^{Zn}

To a Schlenk tube, 60 mg of **2^{Na}** and 2 mL 2.0 M aqueous solution of $Zn(NO_3)_2$ were added. The Schlenk tube was then immersed in the oil bath and incubated at 80 °C for 4 h. Subsequently, the crystals were collected via vacuum filtration, and the aforementioned ion exchange experiment was repeated every 4 hours for a total of 5 cycles until no free Na^+ was detected by ICP-MS. The final product was collected, washed with water, and dried under vacuum at 120 °C to afford **2^{Zn}** as a white free-flowing powder.

ICP measurement indicated the molar ratio of Zn:B:Zr is about 0.55:1:2.77.

IR (KBr, cm^{-1}): 1655 (w), 1590 (w), 1497 (w), 1403 (s), 1280 (w), 1242 (w), 1190 (m), 1035 (m), 763 (m), 721 (w), 644 (s), 589 (w), 518 (w), 453 (s).

2.5 Chemical stability

The activated **2^{Na}**, 100 mg for each batch, was immersed in about 50 mL aqueous solution of 1 M HCl, 1 M NaOH, and 1 mM K_3PO_4 at room temperature for 24 h, respectively. The treated samples were then filtered, washed with DI water (3 times), acetone (3 times), and dried under vacuum at 100 °C for 10 h before PXRD, gravimetric analysis, ^{11}B NMR, and N_2 sorption measurements.

The recoveries after the vacuum drying were 106, 97, and 96 mg, respectively.

2.6 Synthesis of $Na^+B(PhCOOMe)_4^-$

To a flask, lithium tetrakis (4-(methoxycarbonyl) phenyl) borate (1.12 g, 2.0 mmol) was suspended in 50 mL water. Sodium chloride (2.3 g, 40 mmol) was added to this suspension, and then stirred at room temperature overnight. The exchanged $Na^+B(PhCOOMe)_4^-$ was collected by filtration, and the above ion-exchange operation was repeated four times to ensure the complete exchange of Li ions. The final exchanged $Na^+B(PhCOOMe)_4^-$ was collected by filtration and dried under vacuum.

2.7 Weighing analysis of $\mathbf{2^{Na}}$

$\mathbf{2^{Na}}$ was first subjected to Soxhlet extraction using methanol as the eluent for comprehensive purification. After that, $\mathbf{2^{Na}}$ was then degassed under vacuum at 160 °C for 10 h to ensure the complete removal of residual solvent molecules within the framework. The activated sample was then weighed to determine its dry mass (m_0).

The activated $\mathbf{2^{Na}}$ was immersed in DI water for 24 h under ambient conditions. The hydrated sample was subsequently filtered and dried in an oven at 65°C for 12 hours to afford a free-flowing powder, which was then weighed to determine its mass (m_1). The water content in the pore was calculated via mass differential analysis ($\Delta m = m_1 - m_0$), and the water percentage content was then expressed as: $H_2O\% = (m_1 - m_0)/m_0 \times 100$.

The free-flowing powder was then placed at room temperature and weighed again after one week (t_1) and one month (t_2) to calculate the water loss within the pore. The water loss was expressed as: $Water\ loss\ (\%) = [(m_1 - m_t)/(m_1 - m_0)] \times 100$.

2.8 Chemical stability

The activated $\mathbf{2^{Na}}$, 100 mg for each batch, was immersed in about 50 mL aqueous solution of 1 M HCl and 1 M NaOH at room temperature for 24 h, respectively. The treated samples were then filtered, washed with DI water (3 times), acetone (3 times), and dried under vacuum at 100 °C for 10 h before PXRD, gravimetric analysis, ^{11}B NMR, and N_2 sorption measurements. The recoveries after the vacuum drying were 97.1 and 96.6 mg, respectively.

2.9 ICP-MS analysis

5.000 mg $\mathbf{2^{Na}}$ was digested with 10 mL aqua regia in a small beaker, then diluted by 10 wt% HNO_3 and transferred to a volumetric flask. washed the beaker three times, and then diluted with dilute nitric acid to 100 mL for ICP measurement.

$\mathbf{2^{K}}$ and $\mathbf{2^{Zn}}$ were digested in the same manner.

3 Electrochemical measurements

3.1 Cyclic voltammetry (CV) measurement of $\mathbf{2^{Na}}$

Under a force of 5 MPa, 50 mg $\mathbf{2^{Na}}$ was compressed into a pellet with a diameter ranging from 1.0 to 1.4 mm. Subsequently, the pellet was assembled into an airtight Swagelok-type cell to form an asymmetric SS|$\mathbf{2^{Na}}$|Na cell, which was then employed to perform the cyclic voltammetry (CV) measurement at a scan rate of 0.1 mV/s with a voltage range from –0.5 to 5.0 V (vs. Na/Na^+) at room temperature.

3.2 Linear sweep voltammograms (LSV) measurement of 2^{Na}

The linear sweep voltammetry (LSV) measurement was conducted with the asymmetric Na|$\mathbf{2}^{Na}$|Cu, Na|$\mathbf{2}^{Na}$|SS, Na|$\mathbf{2}^{Na}$|Mo, and Na|$\mathbf{2}^{Na}$|Ti cells under a sweep rate of 0.1 mV/s in a voltage range from 0 V to 5.0 V (vs. Na/Na^+) at room temperature.

3.3 Ionic conductivity of 2^{Na}

50 mg $\mathbf{2}^{Na}$ was ground into a fine powder and then pressed into a thin pellet with a thickness of 1.0 to 1.4 mm under a force of 5 MPa. The final thickness of the pellet was measured with a vernier caliper, and the pellet was then sealed in an airtight Swagelok-type cell between two stainless steel blocking electrodes to form a symmetric SS|$\mathbf{2}^{Na}$|SS cell for ionic conductivity measurement.

The alternating current (AC) impedance analysis was performed using a two-probe method with an Autolab AUT88031 potentiostat/galvanostat over the frequency range of 10^{-2} to 10^6 Hz, with an input voltage amplitude of 100 mV. Data was recorded every 10 °C between –40 to 120 °C. Each temperature was held for 1 h to reach thermal equilibrium. At each temperature point, the ionic conductivities (σ) were determined according to the following equation:

$$\sigma = \frac{L}{AR} \qquad (1)$$

where L and A represent the thickness (cm) and the area (cm^2) of the pellet, respectively. And R, which was extracted directly from the impedance plots, is the bulk resistance of the sample (Ω). The activation energy (E_a) was calculated with the Nernst-Einstein relation:

$$\sigma = \frac{\sigma_0}{T} exp(-\frac{E_a}{kT}) \qquad (2)$$

where σ_0 is a pre-exponential factor, T is the temperature, E_a is the activation energy, and k is the Boltzmann constant.

3.4 Electrical conductivity of 2^{Na}

Direct current (DC) polarization measurements were carried out to determine the electronic conductivity. 50 mg $\mathbf{2}^{Na}$ was ground into a fine powder and then pressed into a thin pellet with a thickness of 1.0 to 1.4 mm under a force of 5 MPa. The final thickness of the pellet was measured with a vernier caliper, and the pellet was then sealed in an airtight Swagelok-type cell between two stainless steel blocking electrodes to form a symmetric SS|$\mathbf{2}^{Na}$|SS cell for electronic conductivity measurement. The cells were connected to the Autolab AUT88031 potentiostat/galvanostat in combination with a low-current option. Measurements were recorded at a constant voltage of 2 V, and the currents were recorded for 2000 s The electronic conductivity was calculated to be 1.16×10^{-9} S/cm.

3.5 Ionic transference number of 2^{Na}

The ionic transference number was evaluated using a potentiostatic polarization method at room temperature. The $\mathbf{2}^{Na}$ pellet assembled into an airtight Swagelok-type cell between two Na foils to form a symmetric Na|$\mathbf{2}^{Na}$|Na cell. The direct current (DC) polarization measurement was performed on this cell using an Autolab AUT88031 potentiostat/galvanostat with an applied polarized voltage at 10 mV. The AC impedance of the symmetric cell was conducted over the frequency range 1 MHz–1 Hz, with

an input voltage amplitude of 100 mV. The ionic transference number t was determined according to the following equation:

$$t = \frac{IS(\Delta V - I0R0)}{I0(\Delta V - ISRS)} \qquad (3)$$

where I^S is the steady-state current, I^0 is the initial current, ΔV is the applied potential, R^0 and R^S are the interfacial resistances before and after the polarization, respectively.

3.6 Galvanostatic cycling measurements

Galvanostatic cycling measurement was performed on the asymmetric Na|$\mathbf{2^{Na}}$|Cu cell assembled in the CR2025 button cell. Galvanostatic cycling for this asymmetrical cell was performed using a multichannel battery testing system (LAND CT3001A) by sequentially charging and discharging.

The galvanostatic cycling measurement of the symmetric Na|$\mathbf{2^{Na}}$|Na cell was similar, and this symmetric cell was also assembled in the CR2025 button cell.

3.7 Galvanostatic charge/discharge measurements of the quasi-solid RSB

The $\mathbf{2^{Na}}$ electrolyte was prepared by making a slurry containing $\mathbf{2^{Na}}$: poly(vinylidene difluoride) (PVDF) in the weight ratio of 60:40 in 1-methyl-2-pyrrolidinone (NMP). The slurry was then cast onto stainless steel foil, followed by drying at 85 °C in a vacuum oven for 12 h.

The cathode CityU-36 for RSB was prepared according to the literature *J. Am. Chem. Soc.* **2025**, *147*, 26069–26078. The cathode TQBQ-COF for RLB and RPB was prepared according to the literature *J. Am. Chem. Soc.* **2023**, *145*, 5105−5113. The cathode $NH_4V_4O_{10}$ for RZB was prepared according to the literature *J. Am. Chem. Soc.* **2025***, 147,* 23331–23338.

The cathode CityU-36 was prepared from a slurry of CityU-36, Super-P, and PVDF in the weight ratio of 60:30:10 in NMP. The slurry was ground and then carefully coated on the carbon paper. The coated carbon paper was dried at 85 ℃ in a vacuum oven for 12 h, and pressed for 2 min under a pressure of 30 MPa. The weight loading of CityU-36 was about 1~2 mg/cm^2.

The polished Na foil, $\mathbf{2^{Na}}$ electrolyte, and CityU-36 cathode were assembled into a CR2025 coin cell in an argon glove box. After a 6 h rest at 30 °C, the coin cell was measured by a LAND CT3001A instrument. The galvanostatic charge/discharge test was recorded by cycling between 0.1 to 3.0 V vs Na^+/Na with various current densities.

The PTCDA, TiS_2, and MoS_2 cathodes were prepared similarly.

3.8 Calculation of energy density and power density

The energy density and powder density were calculated by following equations:

$$E = \frac{C \times V}{1000 \times M} \qquad (4)$$

$$P = \frac{E}{t} \qquad (5)$$

Where E represents the energy density (Wh/kg). C is the discharge capacity of the battery (mAh). V is the average discharge voltage of the cell (V). M is the total mass (Kg) of cathode, consumed sodium anode, and electrolyte. P represents the power density (Wh kg^{-1}), and t is the time for full discharge (h).

3.9 Calculation of Ions Diffusion Coefficient

The ions diffusion coefficient (Dion) was tested by using galvanostatic intermittent titration technique (GITT) and calculated based on the equation as follows:

$$D_{ion} = \frac{4L^2}{\pi\tau}\left(\frac{\Delta E_s}{\Delta E_\tau}\right)^2 \qquad (6)$$

where τ and s represent the duration of current pulse and relaxation time, respectively. L corresponds to ions diffusion length, which is equal to the thickness of electrode; S is the total contacting area between electrode and electrolyte; $\Delta E\tau$ represents the voltage change induced by the galvanostatic charge/discharge; and ΔEs is the voltage change between two adjacent equilibrium states.

3.10 ICP-MS analysis of the composition of 2^{Na} electrolyte

After the rate performances, we disassembled the Na|$\mathbf{2}^{Na}$|Cu, Na|$\mathbf{2}^{Na}$|Na, and Na|$\mathbf{2}^{Na}$|CityU-36 cells. The $\mathbf{2}^{Na}$ electrolytes were digested in a small beaker with 10 mL aqua regia, diluted by 10 wt% HNO_3, and transferred to a volumetric flask, washed the beaker three times, and then diluted with dilute nitric acid to 100 mL for ICP measurement. ICP-MS measurements indicated the molar ratios of the Na:Zr after the rate performance were 1:3.12, 1:2.99, and 1:3.04, respectively.

Table S1. Crystal data and structure refinement for 2^{Na}.

Identification code	**2^{Na}**
Empirical formula	$C_{58}H_{35}B_2O_{34}Zr_6$
Formula weight	1844.8
Temperature (K)	170
Wavelength (Å)	CuKα (λ = 1.54184)
Crystal system	orthorhombic
Space group	Pnma
Unit cell dimensions	a = 25.1977 (5) Å b = 30.0943 (4) Å c = 17.3014 (3) Å $\alpha = \beta = \gamma = 90$
Volume (Å^3), Z	13120.8 (4), 4
Density (calculated) (mg/m^3)	0.971
Absorption coefficient (mm^{-1})	4.213
F(000)	3780.0
θ range for data collection (º)	7.016 to 132.018
Limiting indices	$-29 \leq h \leq 29$ $-35 \leq k \leq 35$ $-20 \leq l \leq 12$
Reflections collected	35792
Independent reflections	11666 [R_{int} = 0.0415, R_{sigma} = 0.0462]
Completeness to theta	100%
Data / restraints / parameters	11666/0/493
Goodness-of-fit on F^2	1.055
Final R indices [I>2sigma(I)]	R_1 = 0.0606, wR_2 = 0.1730
R indices (all data)	R_1 = 0.0756, wR_2 = 0.1901
Largest diff. peak and hole (e.Å^{-3})	1.68/-0.99

4 Characterization

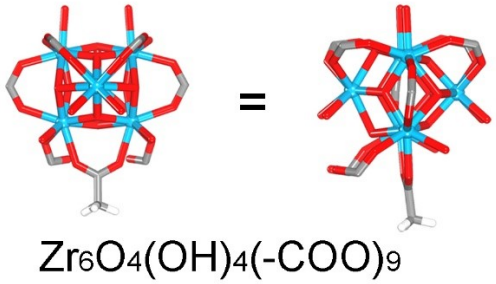

Figure S1. The structure of the Zr_6 cluster

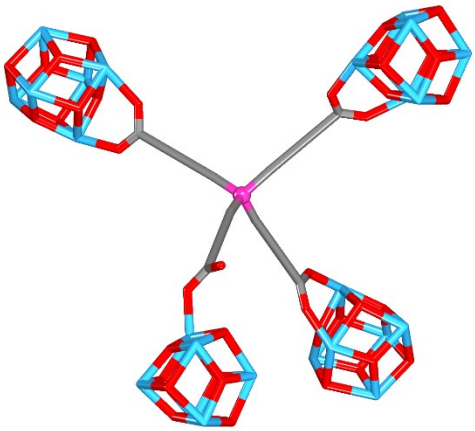

Figure S2. The simplified coordination environments of the ligand

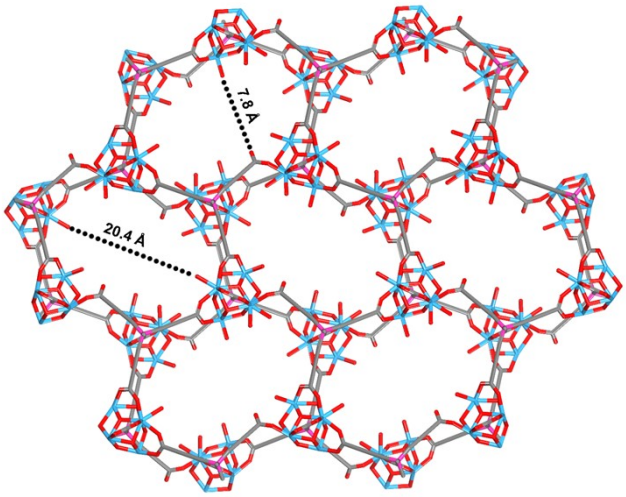

Figure S3. The simplified packing mode of $\mathbf{2}^{\mathbf{Na}}$ viewed along the b-axis

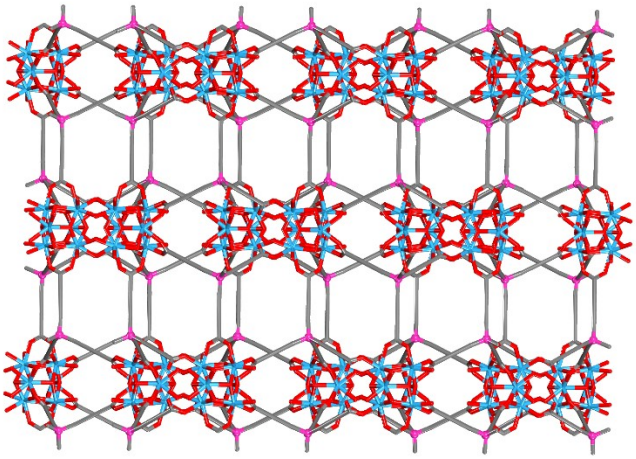

Figure S4. The simplified packing mode of $\mathbf{2}^{\mathbf{Na}}$ viewed along the c-axis

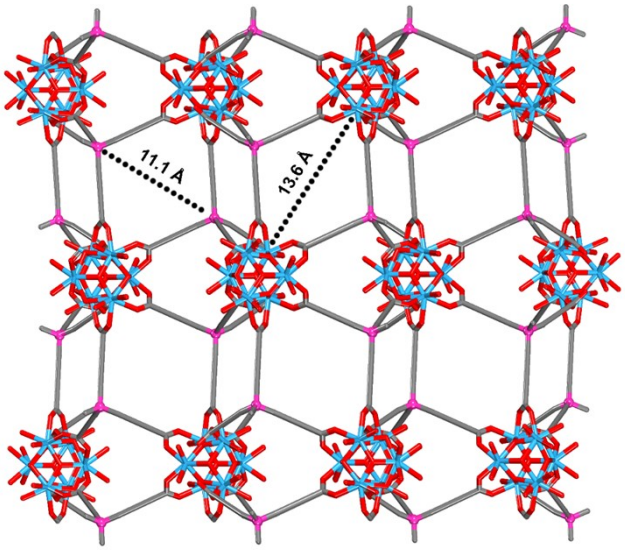

Figure S5. The size of the rhombic windows in $\mathbf{2}^{\mathbf{Na}}$

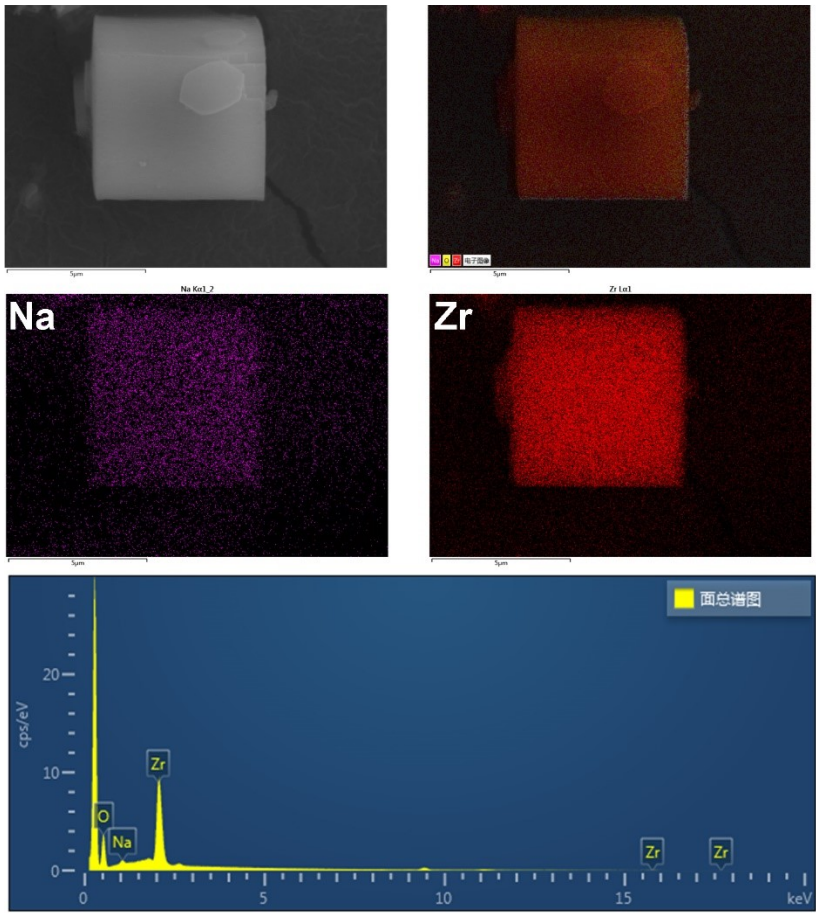

Figure S6. SEM and SEM-EDS mapping of $\mathbf{2^{Na}}$.

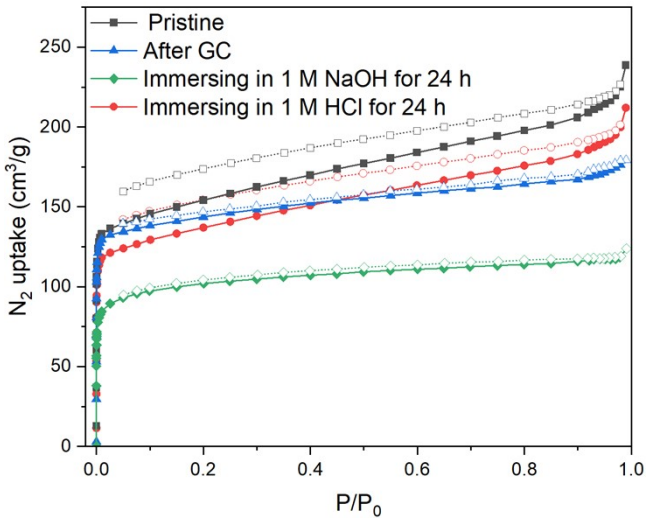

Figure S7. N_2 adsorption isotherms of $\mathbf{2^{Na}}$.

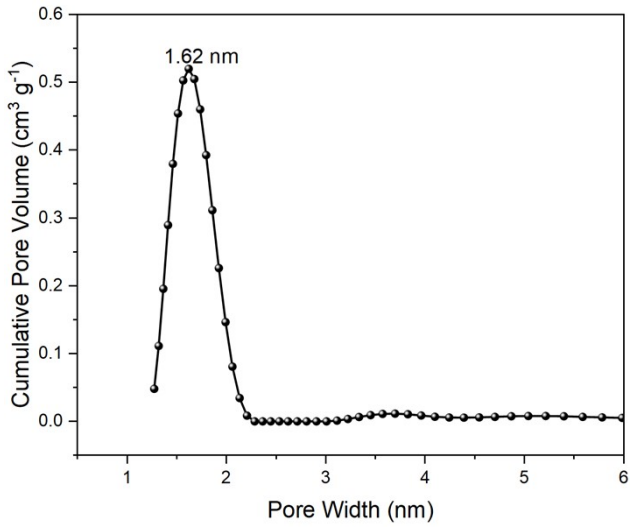

Figure S8. Pore size distribution profiles of **2Na**.

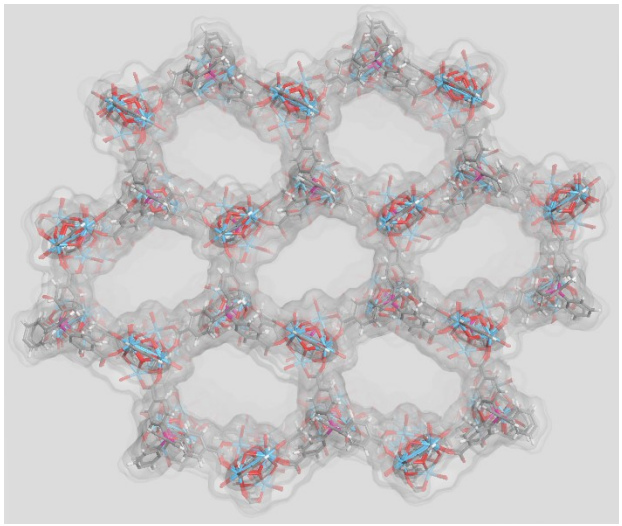

Figure S9. The simulation of the pore size.

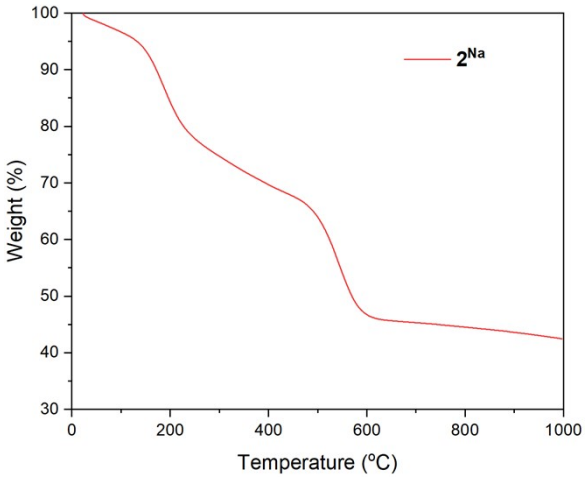

Figure S10. TGA curve.

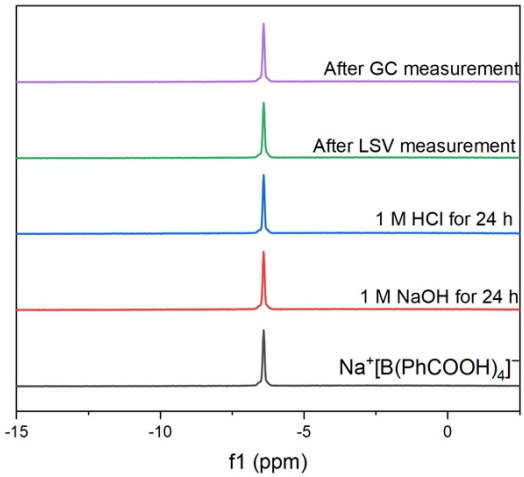

Figure S11. ^{11}B NMR spectra

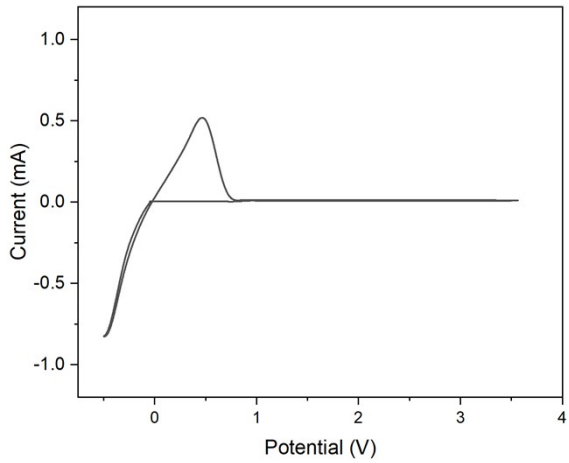

Figure S12. Cyclic voltammetry (CV) test for $\mathbf{2^{Na}}$. CV of $\mathbf{2^{Na}}$ displayed a wide window of electrochemical stability, no significant current flow corresponding to electrolyte decomposition was observed up to 3.5 V. Only cathodic and anodic currents corresponding to Sodium deposition ($Na^+ + e^- \rightarrow Na$) and stripping ($Na \rightarrow Na^+ + e^-$) were observed near –0.5 V vs Na.

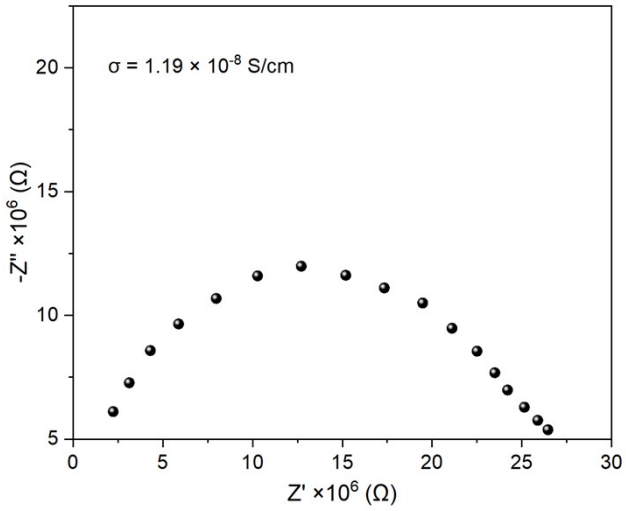

Figure S13. Ionic conductivity of $Na^{+}B(PhCOOMe)_4^{-}$.

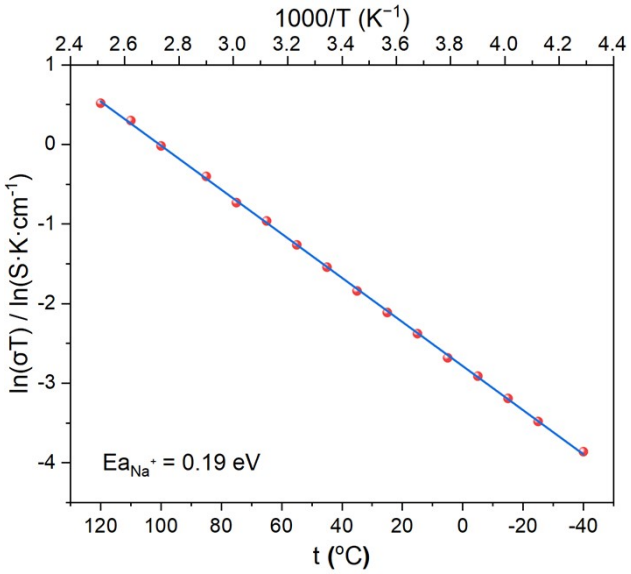

Figure S14. Activation energy of $\mathbf{2^{Na}}$.

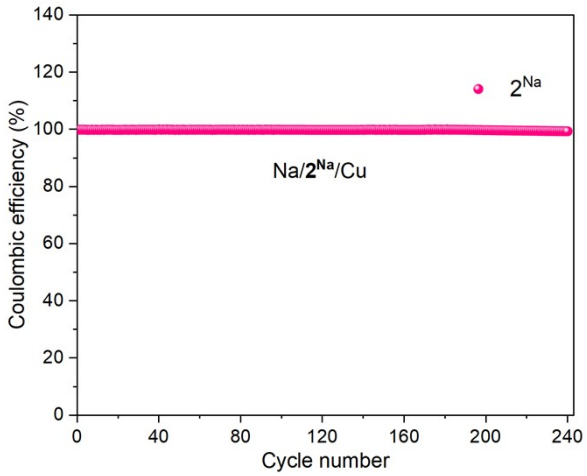

Figure S15. Rate performance of the asymmetric Na|$\mathbf{2^{Na}}$|Cu cell.

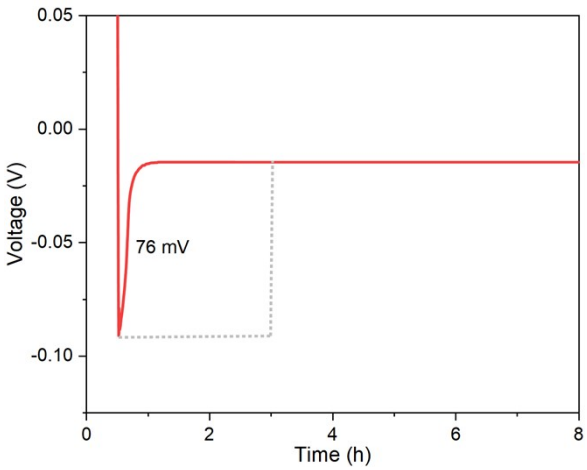

Figure S16. Nucleation overpotential of the asymmetric Na|$\mathbf{2^{Na}}$|Cu cell.

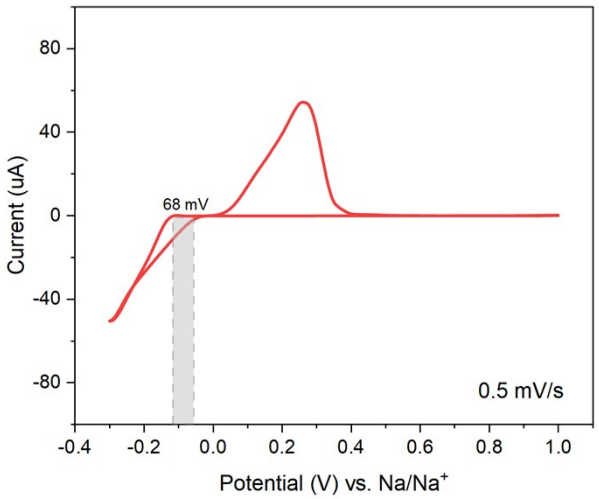

Figure S17. Cyclic voltammetry (CV) measurement of Na|**2**^{Na}|Na cell.

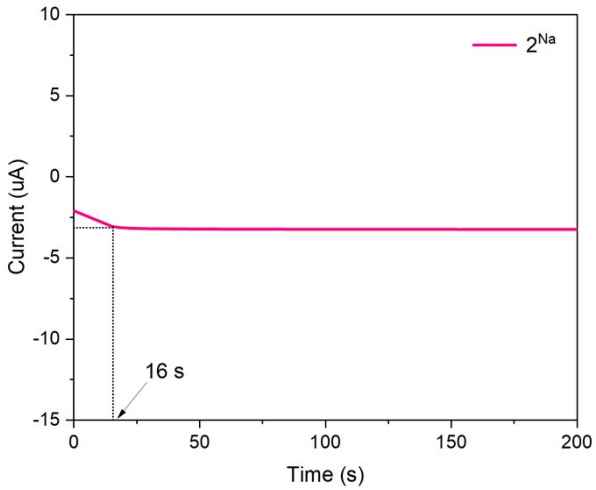

Figure S18. Curves of chronoamperometry for the symmetric Na|**2**^{Na}|Na cell.

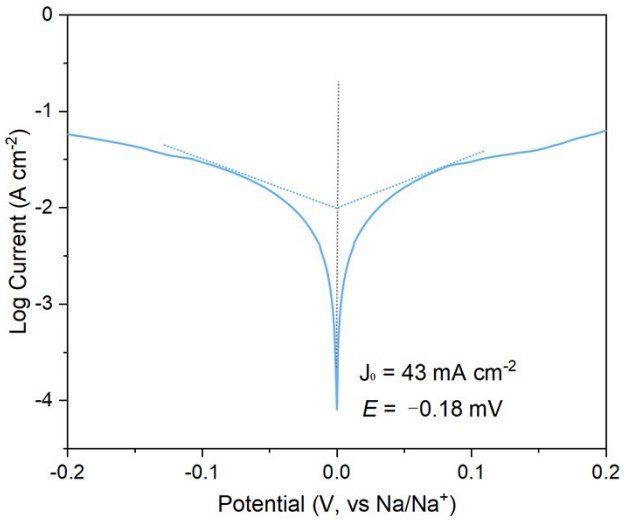

Figure S19. Tafel plots of the symmetric Na|**2**^{Na}|Na cell.

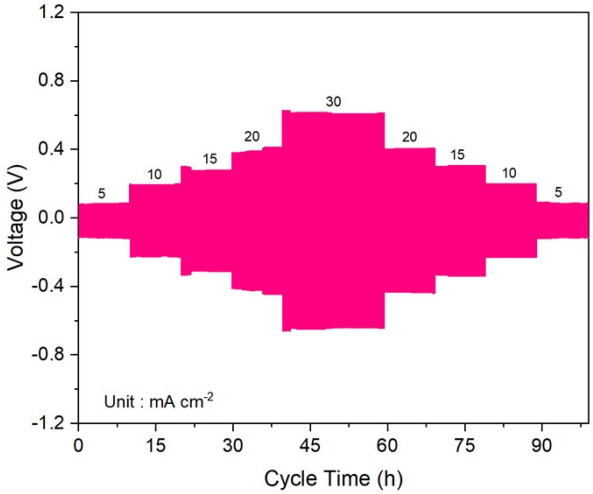

Figure S20. Rate performance of the symmetric Na|**2**^{Na}|Na cell at current densities from 5 to 30 mA/cm^2.

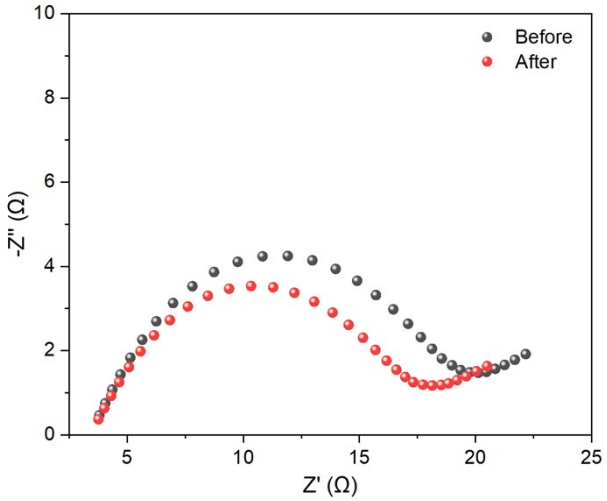

Figure S21. Impedance changes of the symmetric Na|**2**^{Na}|Na cell before and after GC measurement.

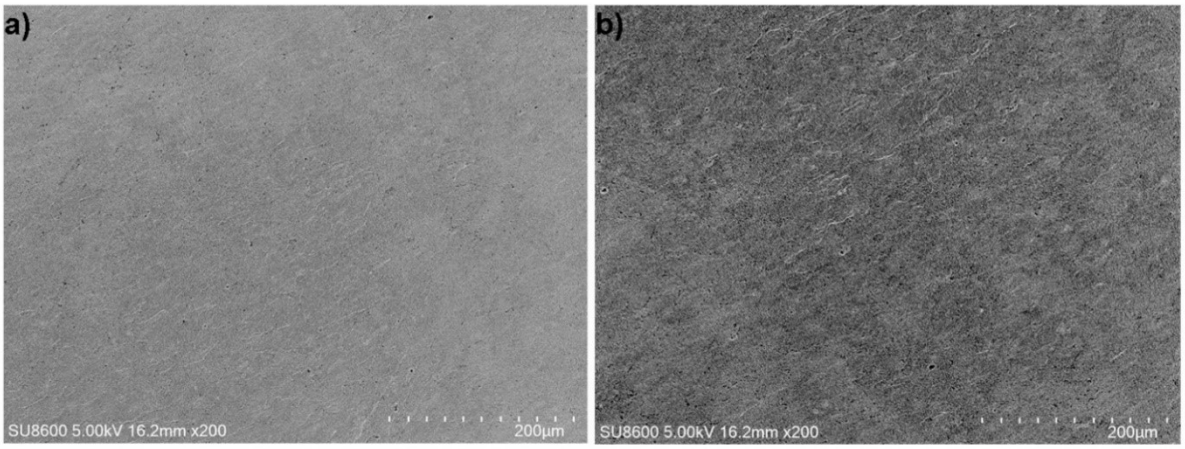

Figure S22. SEM morphology of the Na metal surface before (**a**) and after (**b**) the GC measurement.

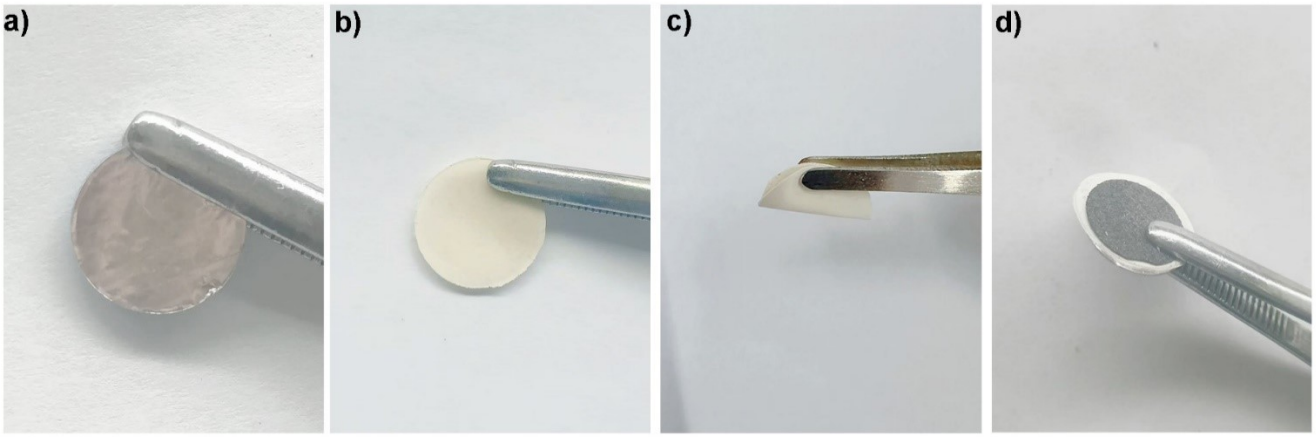

Figure S23. Photograph of the Na metal anode (**a**), **2**^{Na} electrolyte (**b**, **c**), and cathode (**d**) in the coin-type cell.

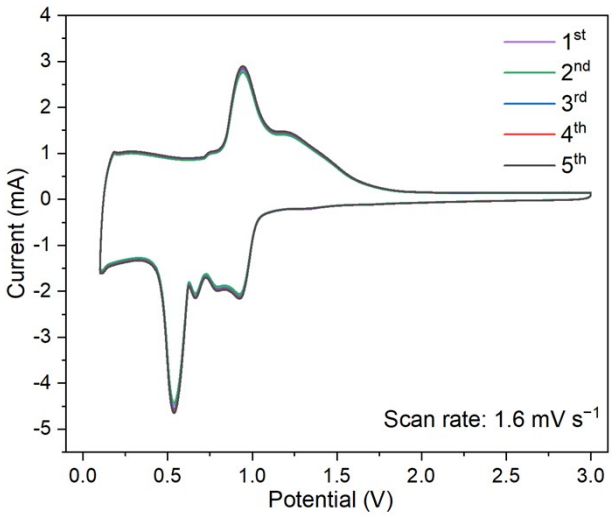

Figure S24. CV curves of the Na|**2**^{Na}|CityU-36 under 1.6 mV s^{-1}

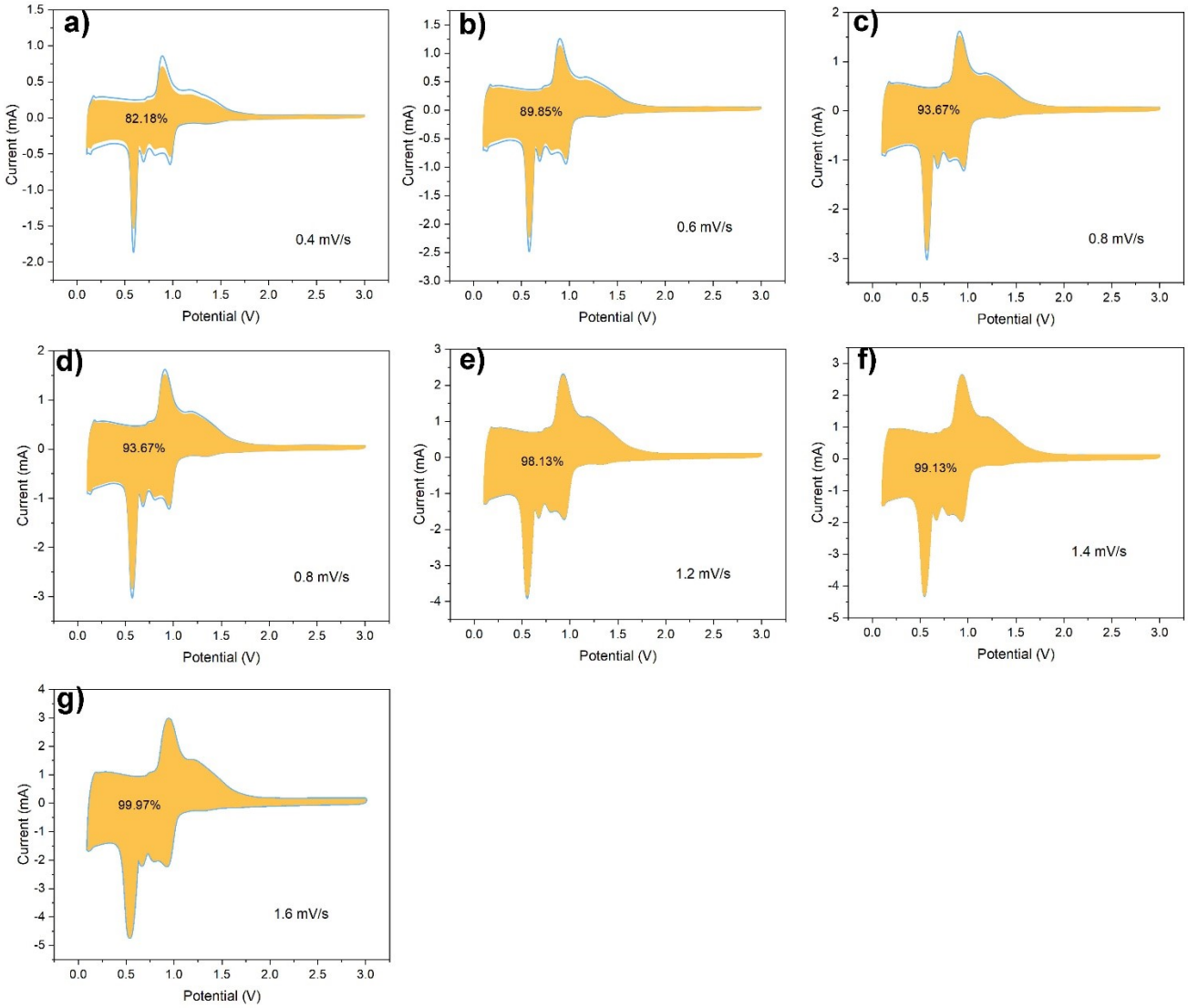

Figure S25. Contribution of the capacitance at various scan rates.

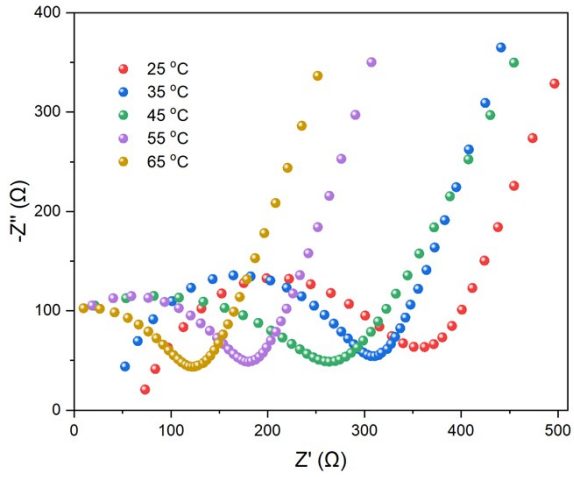

Figure S26. Electrochemical impedance spectroscopy of the Na|**2**^{Na}|CityU-36 at temperatures from 25 to 65 °C.

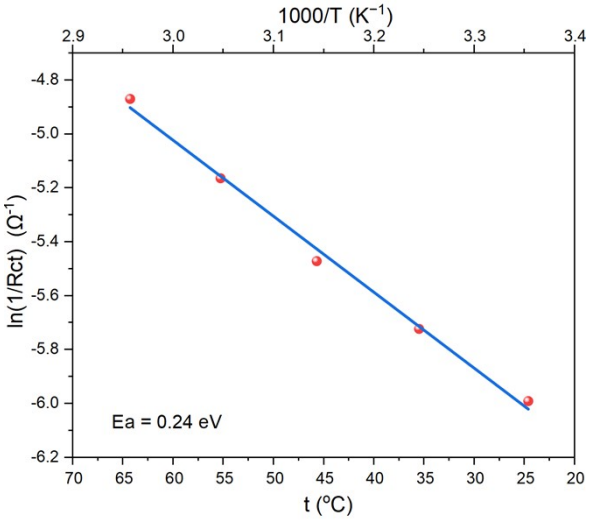

Figure S27. Arrhenius relationships to the operation temperatures for the Na|**2**^{Na}|CityU-36 battery.

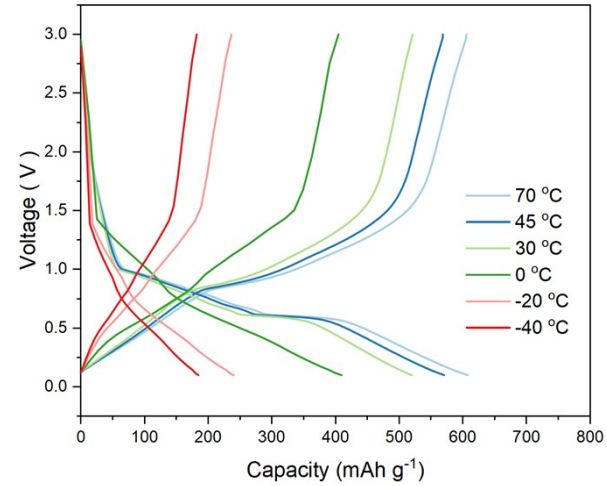

Figure S28. Charge–discharge curves of the Na|**2**^{Na}|CityU-36 battery at 0.1 A/g at different temperature.

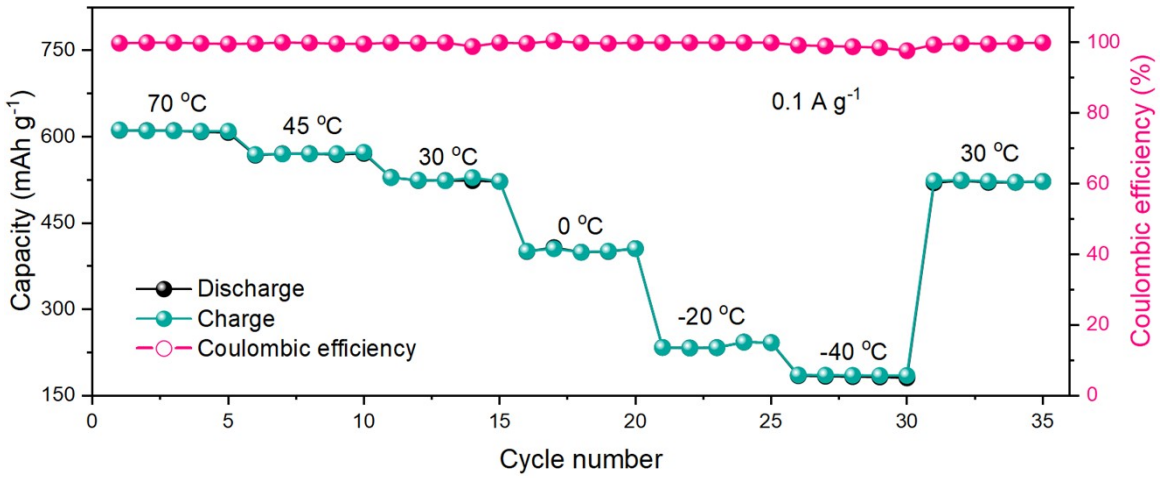

Figure S29. GCD performance of the Na|**2**^{Na}|CityU-36 battery at 0.1 A/g stepwise decrease of temperature from 70 to −40 °C, and then stepwise increase to 30 °C.

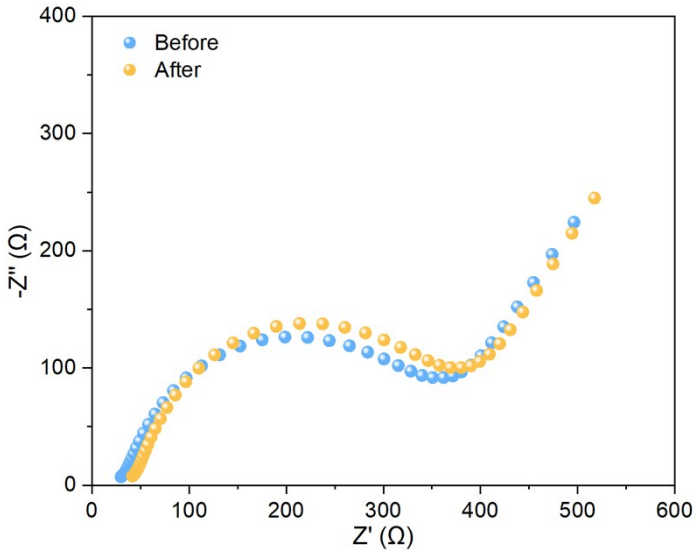

Figure S30 Impedance changes of the Na|**2**^{Na}|CityU-36 during the Long-term GCD measurement at 2 A/g.

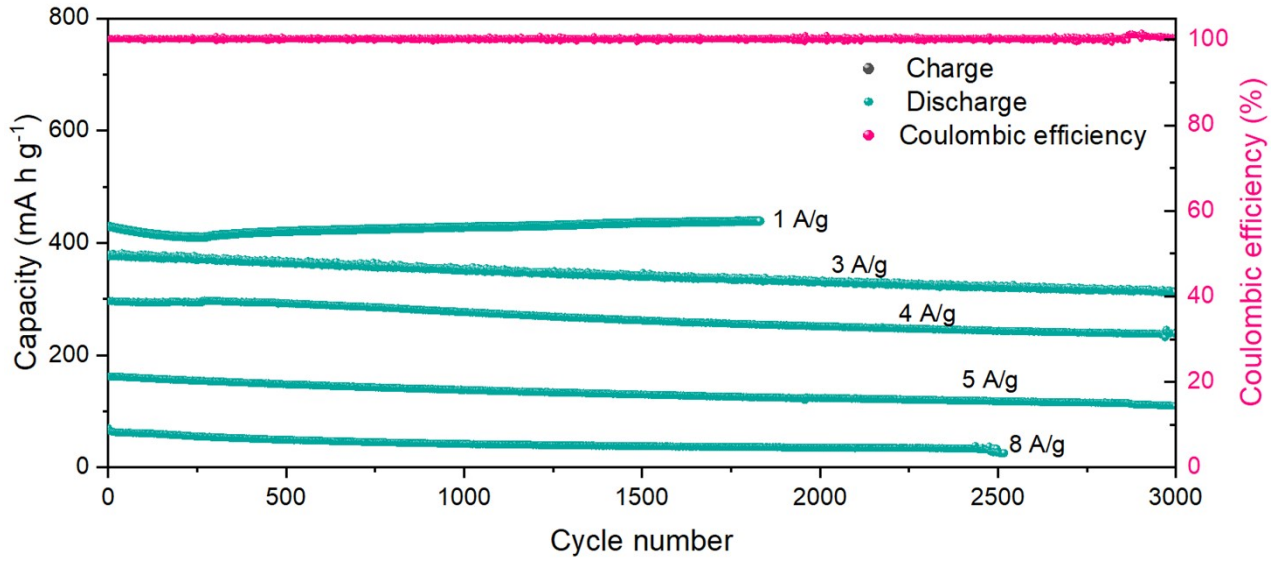

Figure S31. Long-term GCD performance of the Na|**2**^{Na}|CityU-36 battery at 1, 3, 4, 5, and 8 A/g at room temperature, respectively.

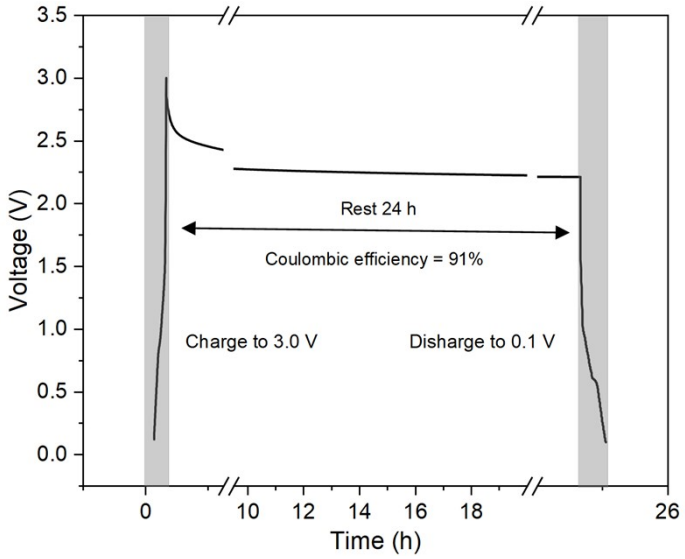

Figure S32. Self-discharge tests of the Na|**2**^{Na}|CityU-36 battery at room temperature.

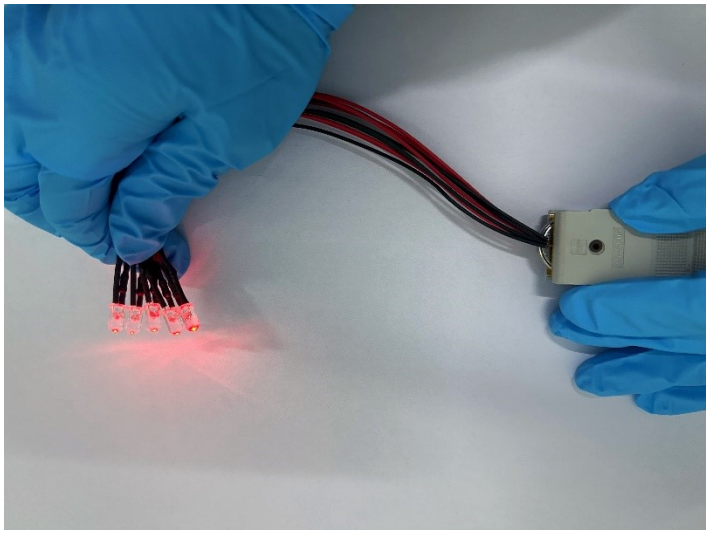

Figure S33. The fabricated solid-state RSB for lighting LED lamps.

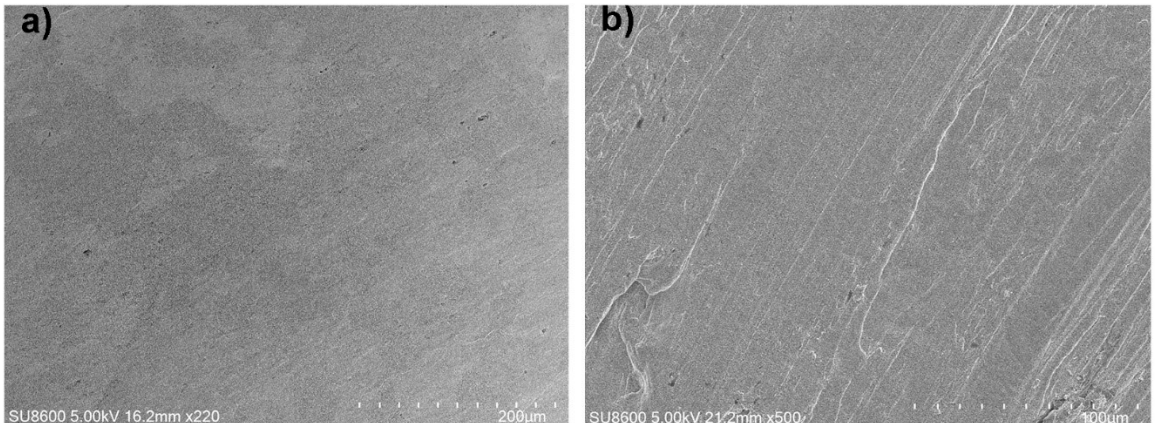

Figure S34. SEM morphology of the Na metal surface before (**a**) and after (**b**) the Long-term GCD measurement.

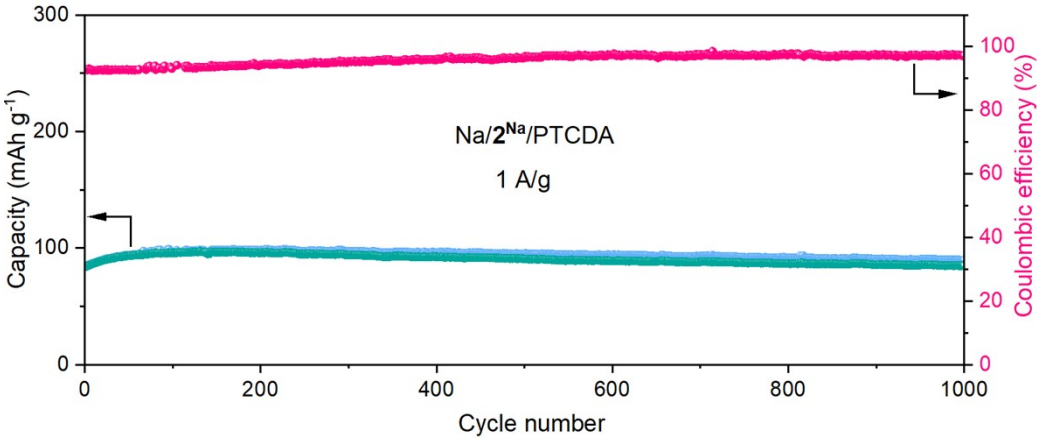

Figure S35. Long-term GCD performance of the Na|**2**^{Na}|PTCDA battery at 1 A/g at room temperature

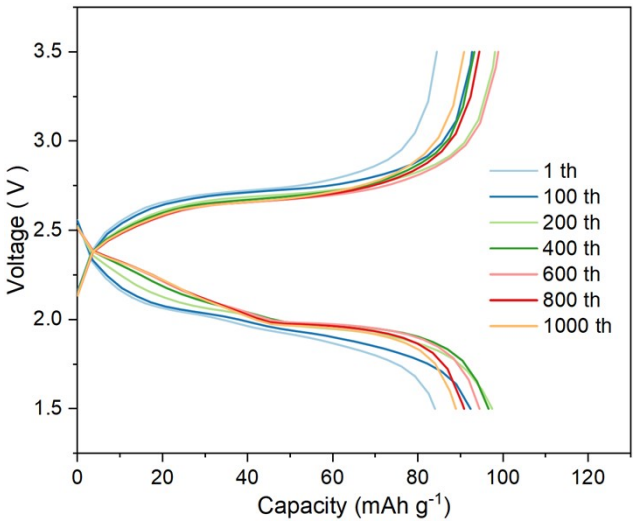

Figure S36. Charge–discharge curves of the Na|**2**^{Na}|PTCDA battery at 1 A/g at room temperature.

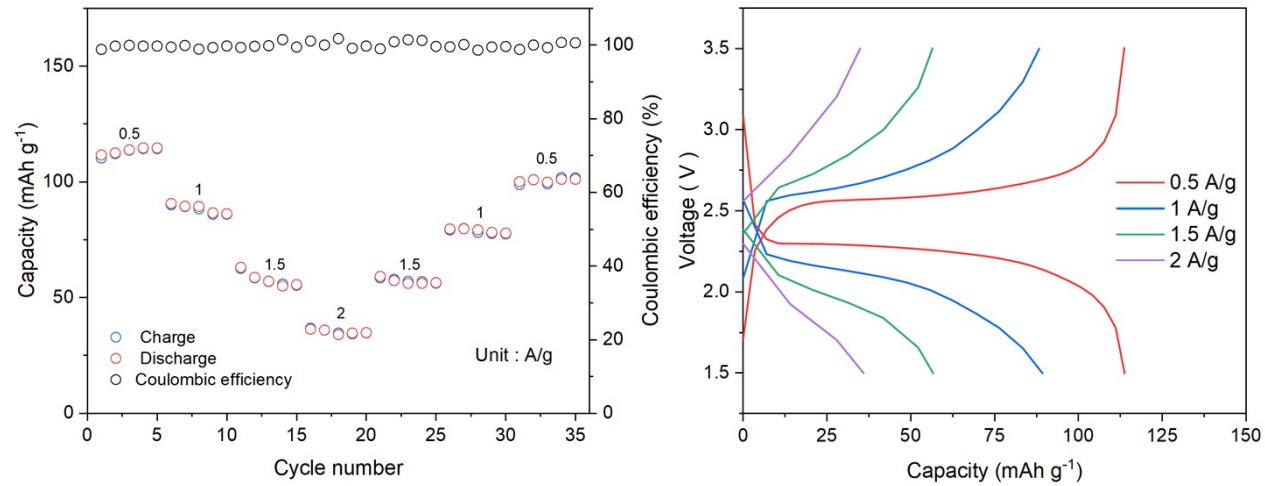

Figure S37. Galvanostatic charge-discharge curves of the Na|**2**^{Na}|PTCDA battery at different rates at room temperature.

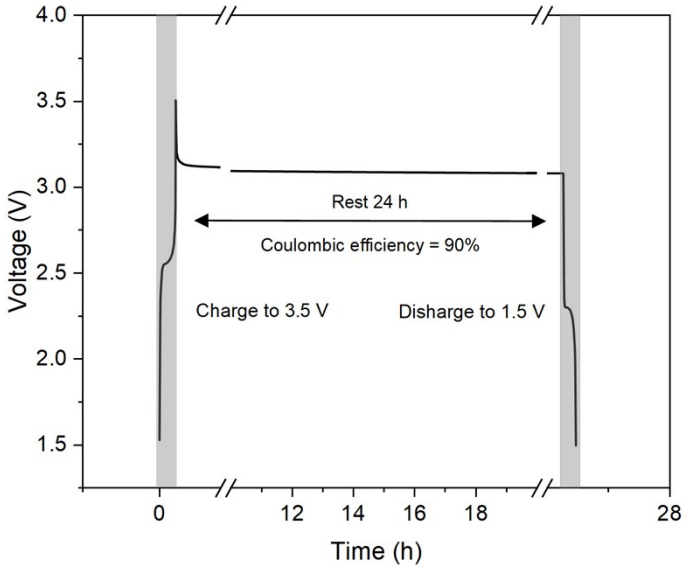

Figure S38. Self-discharge tests of the Na|**2**^{Na}|PTCDA battery at room temperature.

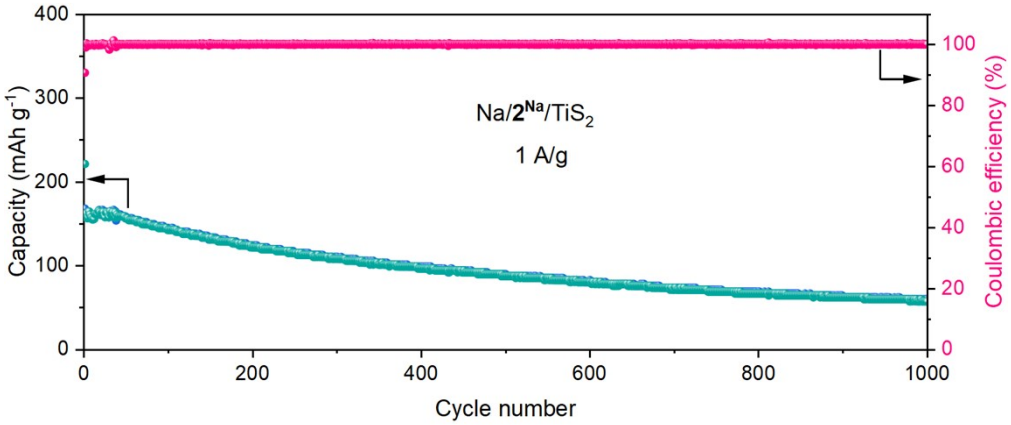

Figure S39. Long-term GCD performance of the Na|**2**^{Na}|TiS_2 battery at 1 A/g at room temperature.

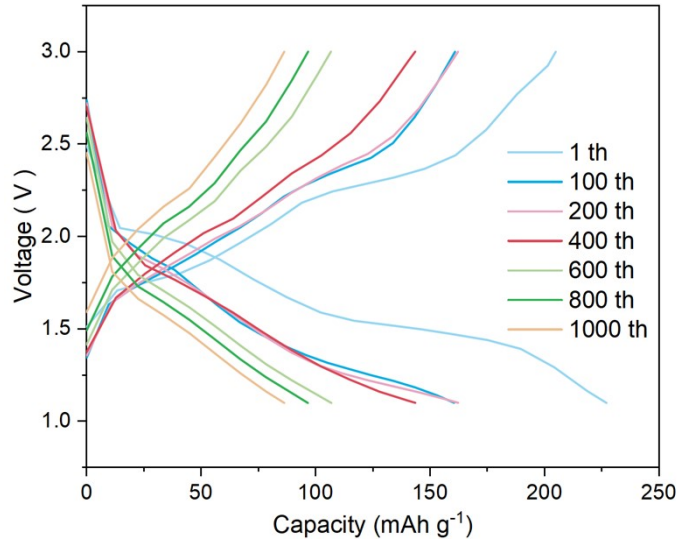

Figure S40. Charge–discharge curves of the Na|**2**^{Na}|TiS_2 battery at 1 A/g at room temperature.

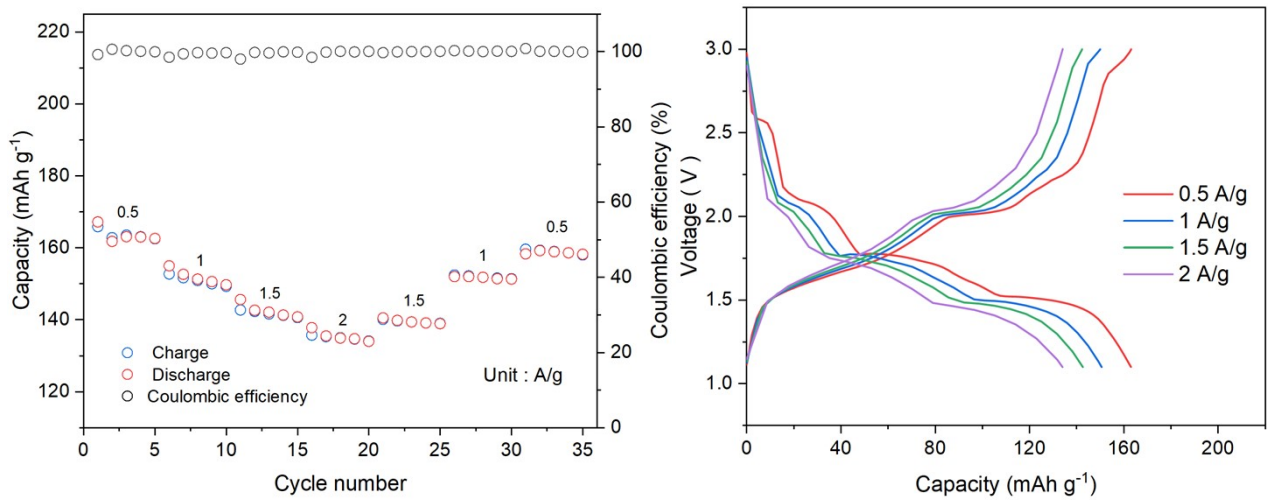

Figure S41. Galvanostatic charge-discharge curves of the Na|**2**^{Na}|TiS_2 battery at different rates

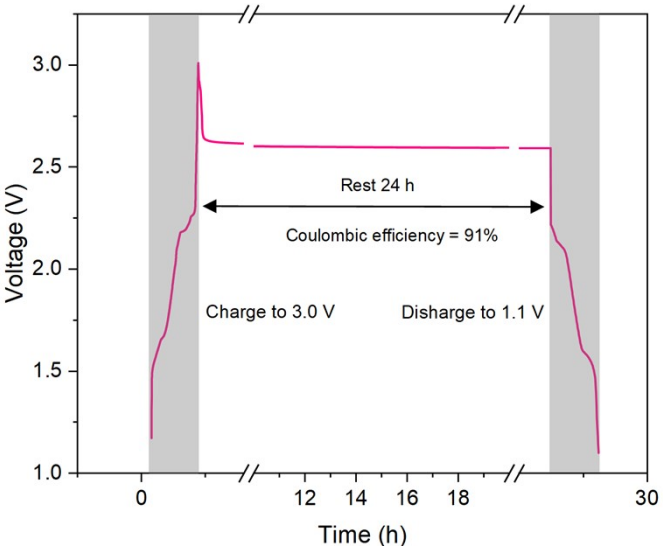

Figure S42. Self-discharge tests of the Na|**2**^{Na}|TiS_2 battery

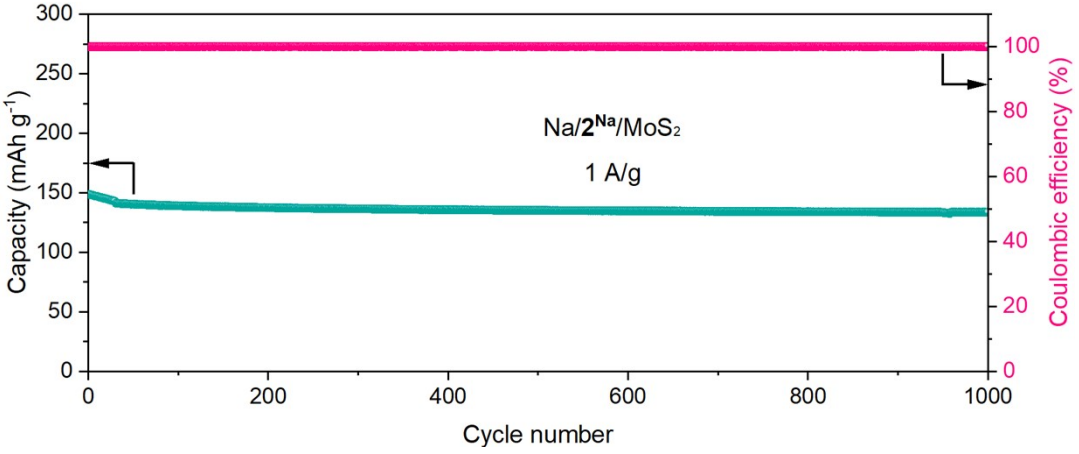

Figure S43. Long-term GCD performance of the Na|**2**^{Na}|MoS_2 battery at 1 A/g at room temperature

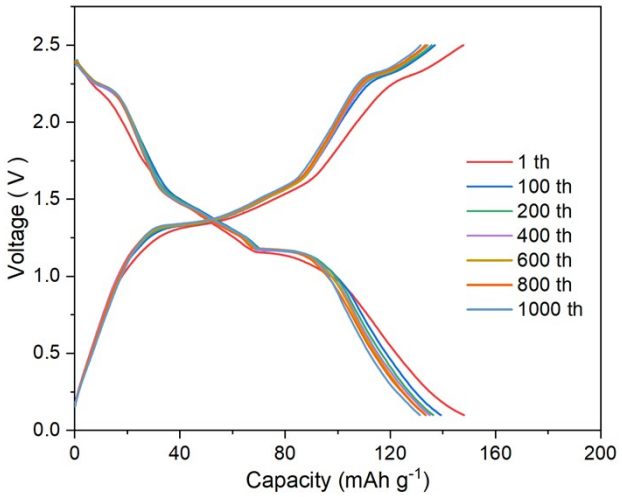

Figure S44. Charge–discharge curves of the Na|**2**^{Na}|MoS_2 battery at 1 A/g at room temperature.

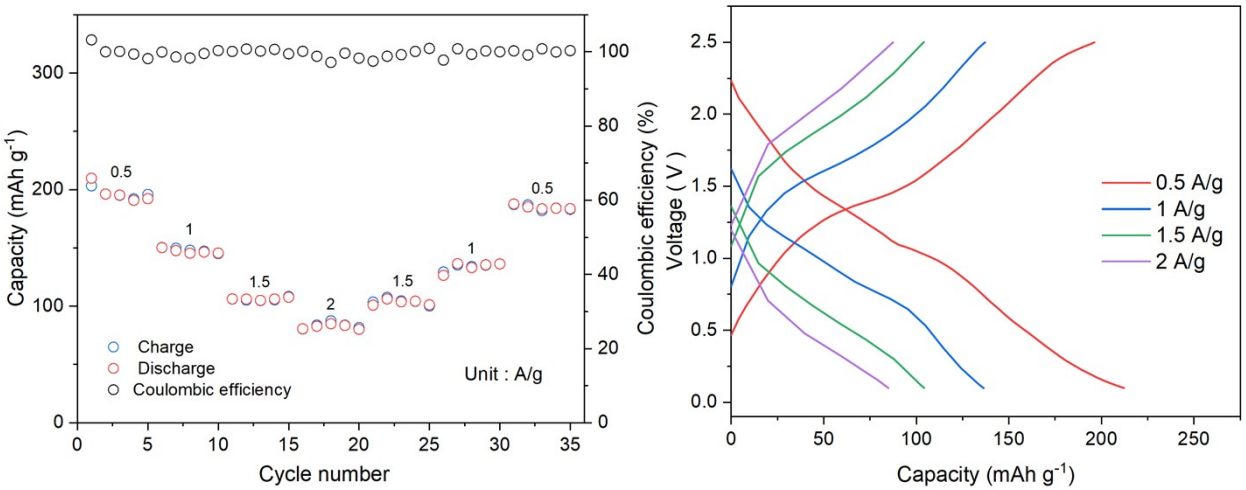

Figure S45. Galvanostatic charge-discharge curves of the Na|**2**^{Na}|MoS_2 battery at different rates.

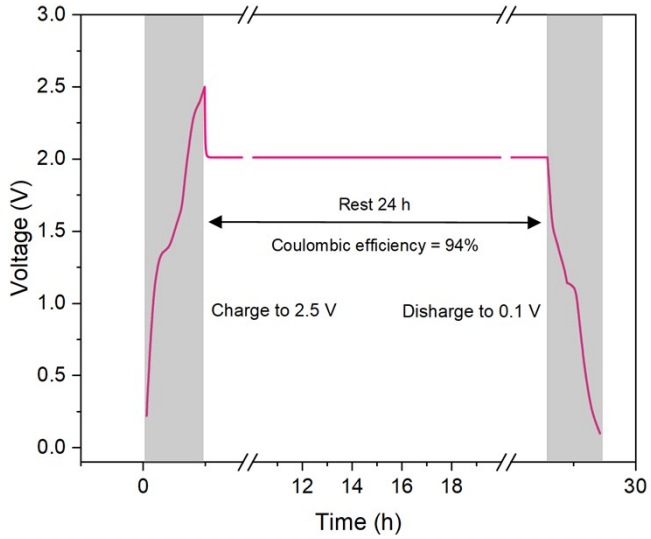

Figure S46. Self-discharge tests of the Na|**2**^{Na}|MoS_2 battery.

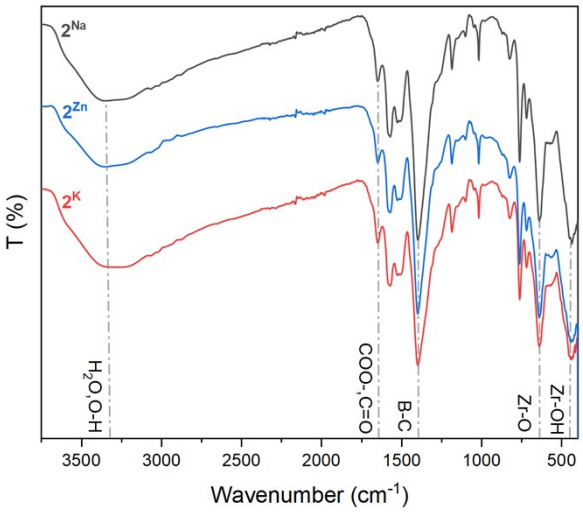

Figure S47. IR spectrum of $\mathbf{2^{K}}$ and $\mathbf{2^{Zn}}$

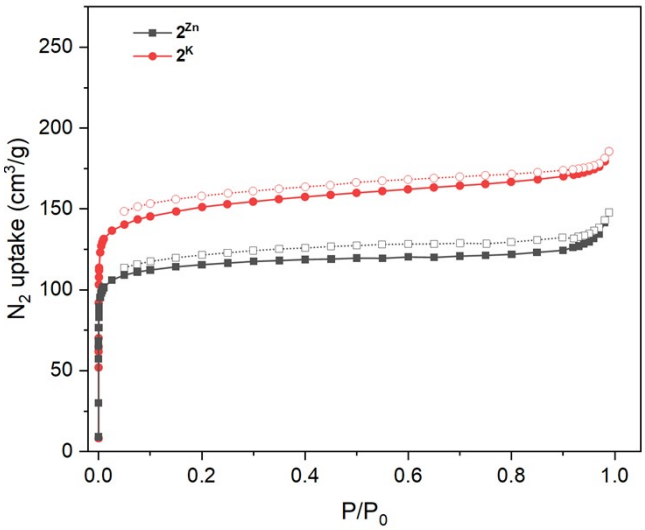

Figure S48. N_2 adsorption isotherms of $\mathbf{2^{K}}$ and $\mathbf{2^{Zn}}$

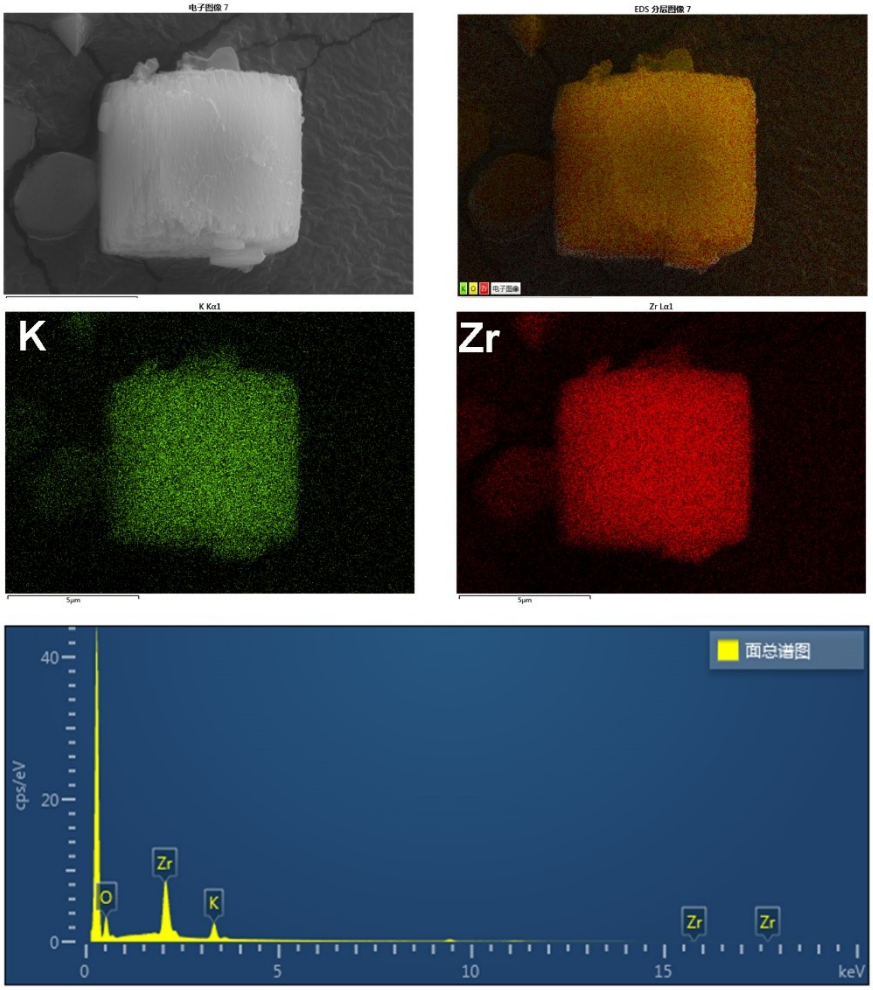

Figure S49. SEM and SEM-EDS mapping of $\mathbf{2^K}$.

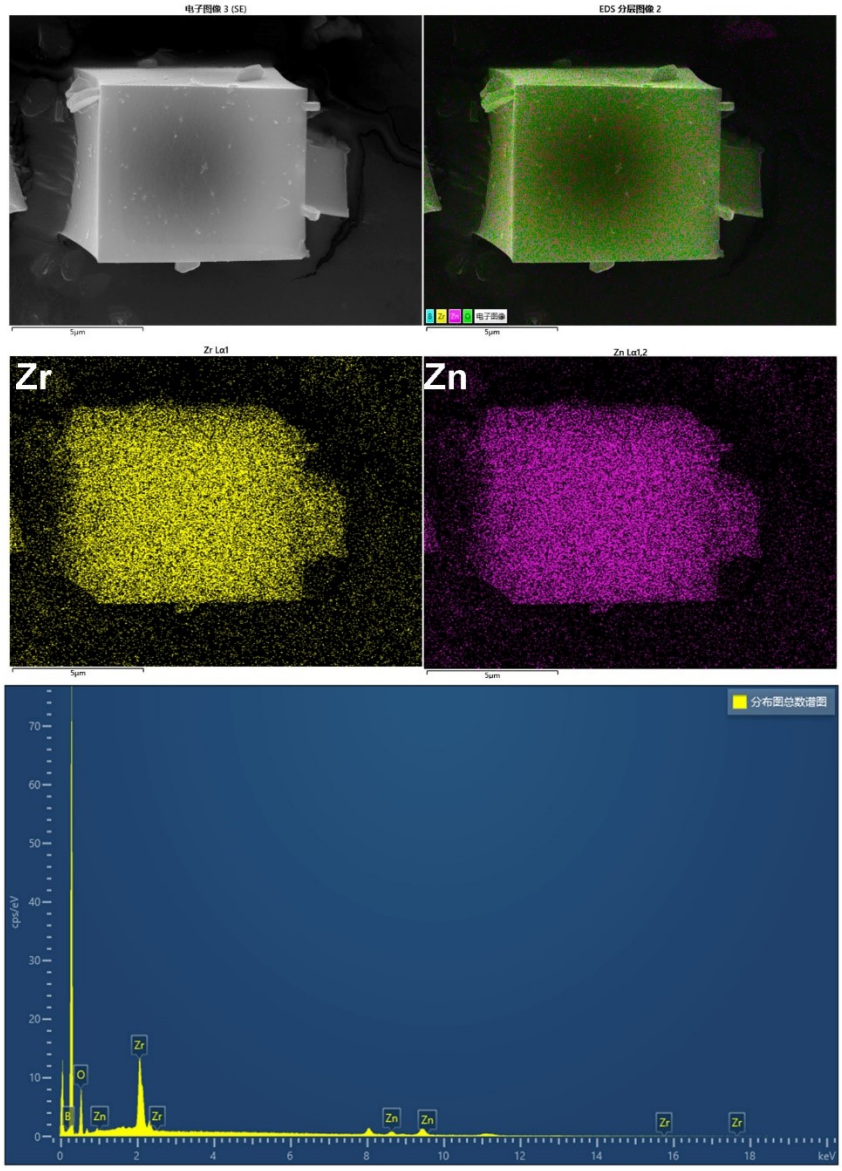

Figure S50. SEM and SEM-EDS mapping of $\mathbf{2^{Zn}}$.

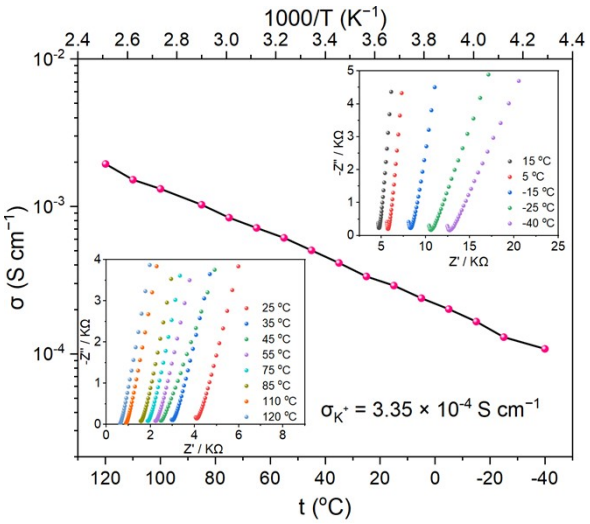

Figure S51. Ionic conductivity of **2^{K}**

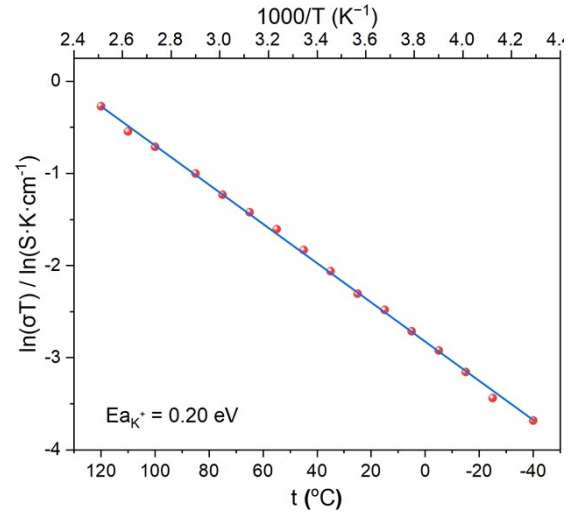

Figure S52. Activation energy of **2^{K}**

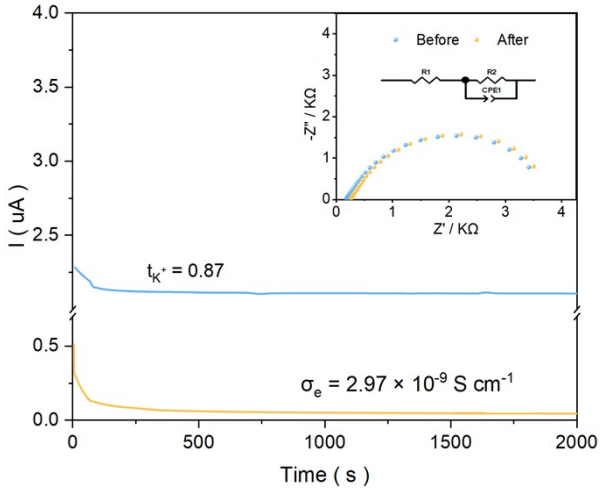

Figure S53. Transference number of **2^{K}**

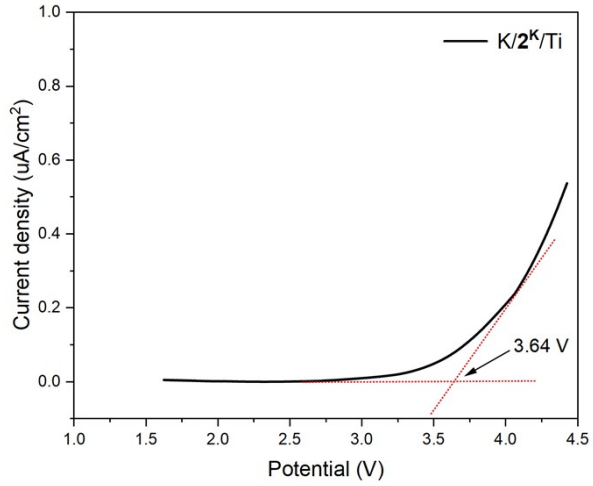

Figure S54. LSV measurements for the K/**2**^{K}/Ti asymmetric cells at room temperature at a scan speed of 0.1 mV s^{-1}

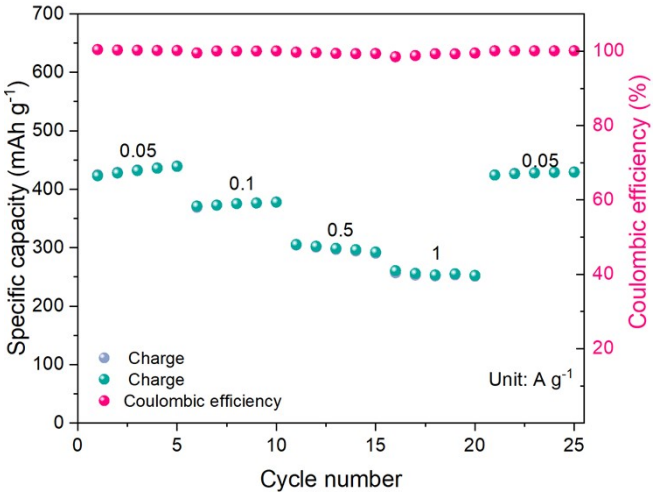

Figure S55. Rate and cycling performance of the K|**2**^{K}| TQBQ-COF at the current density from 0.05 to 1 A g^{-1} at room temperature.

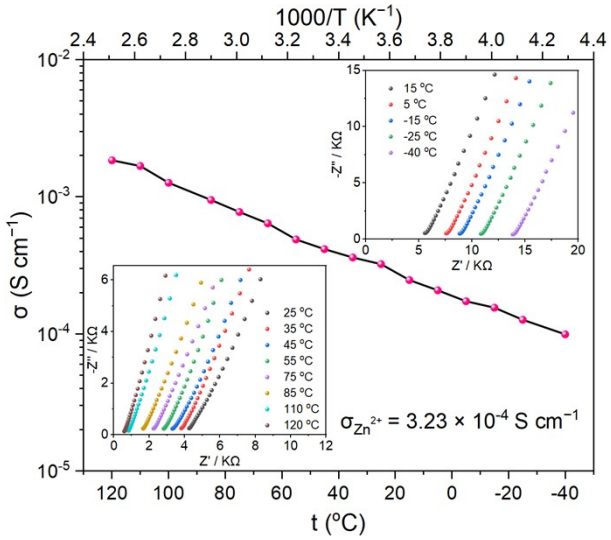

Figure S56. Ionic conductivity of **2**^{Zn}

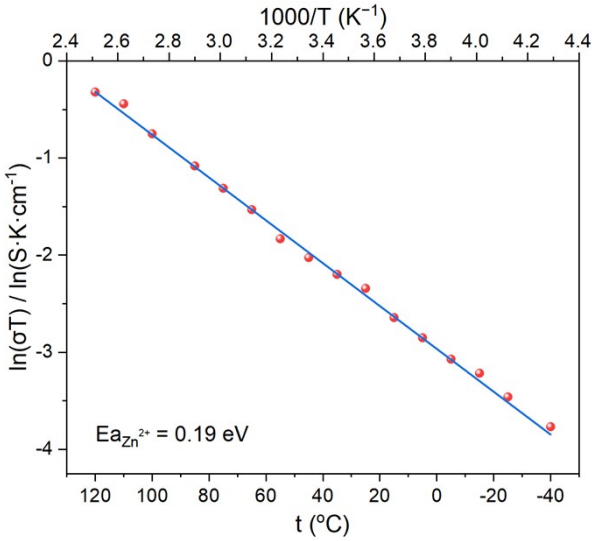

Figure S57. Activation energy of **2^{Zn}**

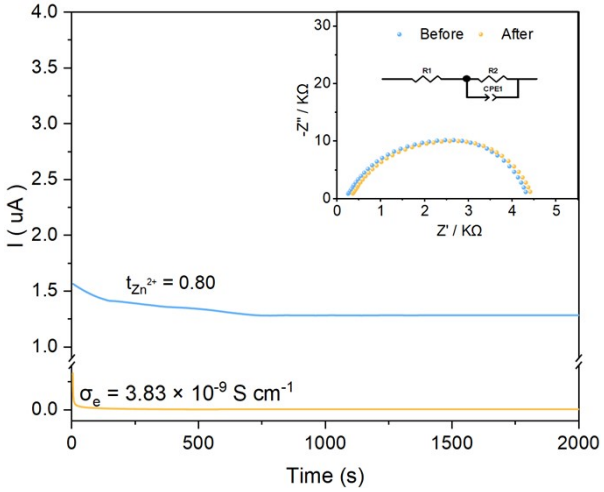

Figure S58. Transference number of **2^{Zn}**

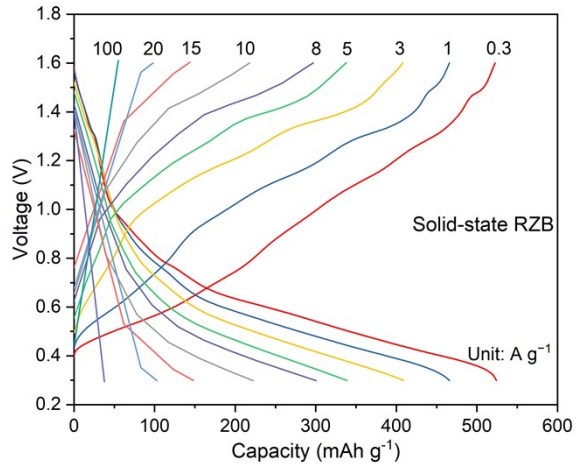

Figure S59. Rate performance of the Zn|**2^{Zn}**|$NH_4V_4O_{10}$ battery at the current density from 0.3 to 100 A/g at room temperature.

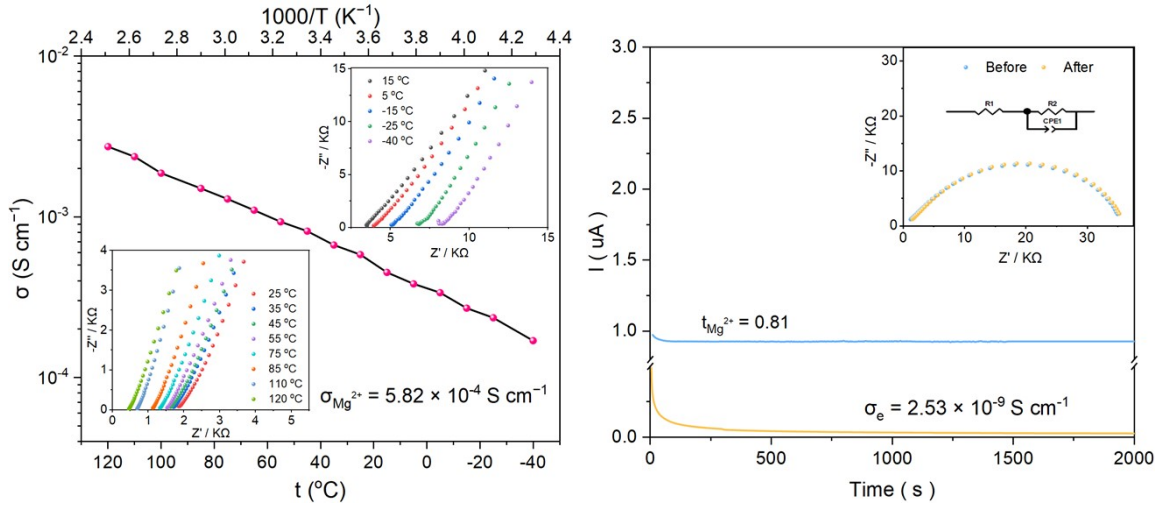

Figure S60. Ionic conductivity and transference number of **2^{Mg}**

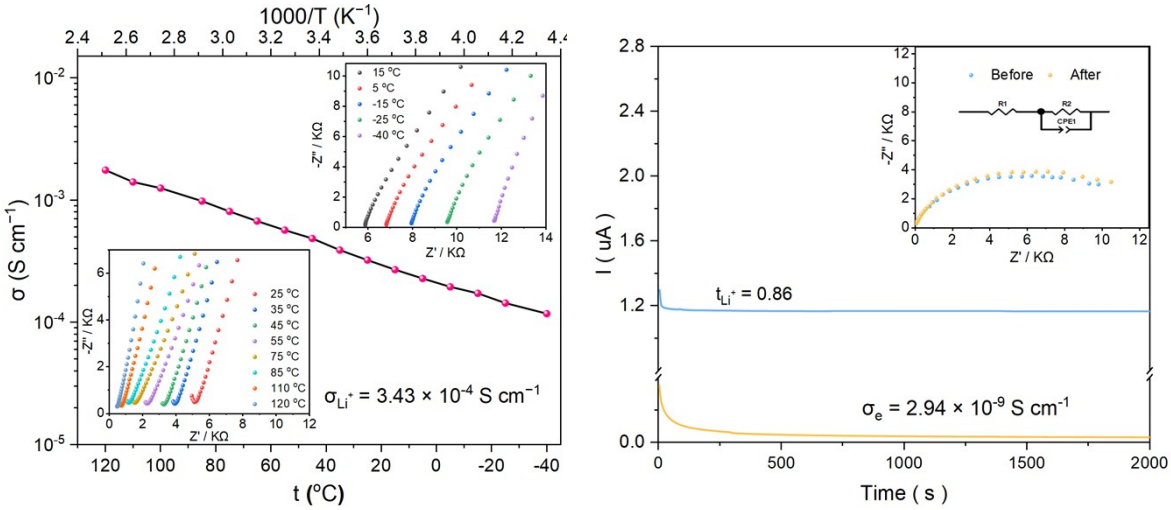

Figure S61. Ionic conductivity and transference number of **2^{Li}**

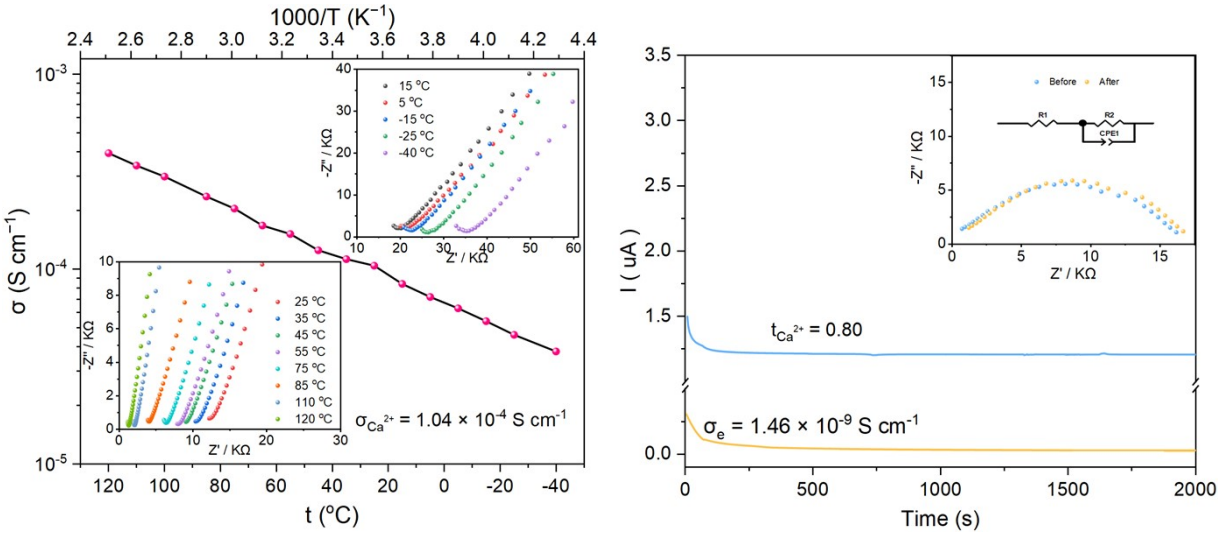

Figure S62. Ionic conductivity and transference number of **2^{Ca}**

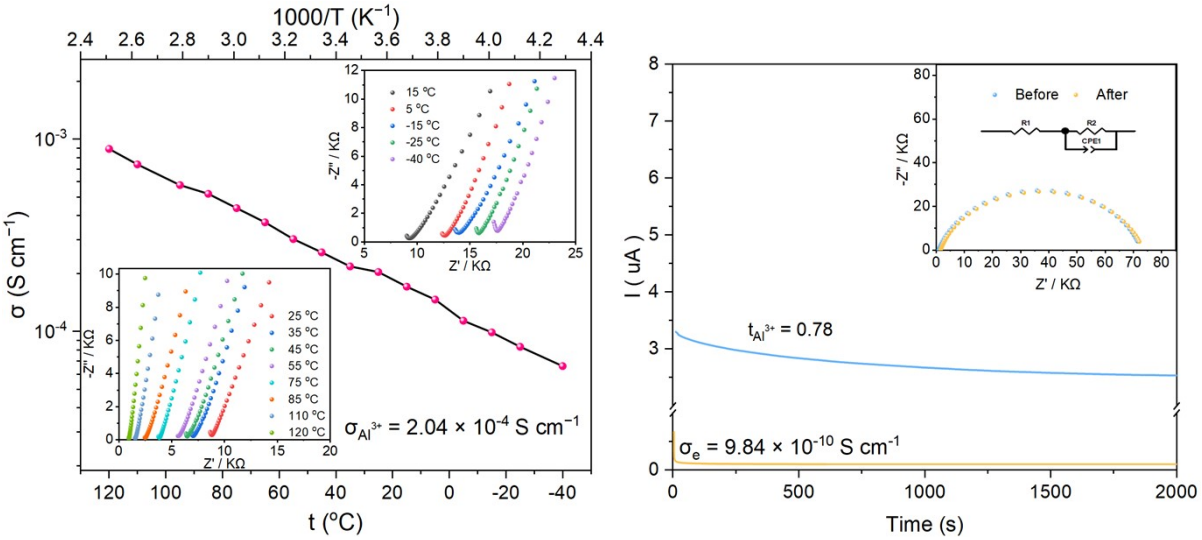

Figure S63. Ionic conductivity and transference number of $\mathbf{2}^{\mathbf{Al}}$

Table S2. Ionic Conductivity, activation energy, and transference number of $\mathbf{2}^{\mathbf{M}}$ at room temperature.

Electrolyte	σ (S/cm)	E_a (eV)	t
$\mathbf{2}^{\mathbf{Li}}$	3.43×10^{-4}	0.17	0.86
$\mathbf{2}^{\mathbf{K}}$	3.35×10^{-4}	0.20	0.87
$\mathbf{2}^{\mathbf{Mg}}$	5.82×10^{-4}	0.18	0.81
$\mathbf{2}^{\mathbf{Ca}}$	1.04×10^{-4}	0.14	0.80
$\mathbf{2}^{\mathbf{Al}}$	2.04×10^{-4}	0.16	0.78
$\mathbf{2}^{\mathbf{Zn}}$	3.23×10^{-4}	0.19	0.80

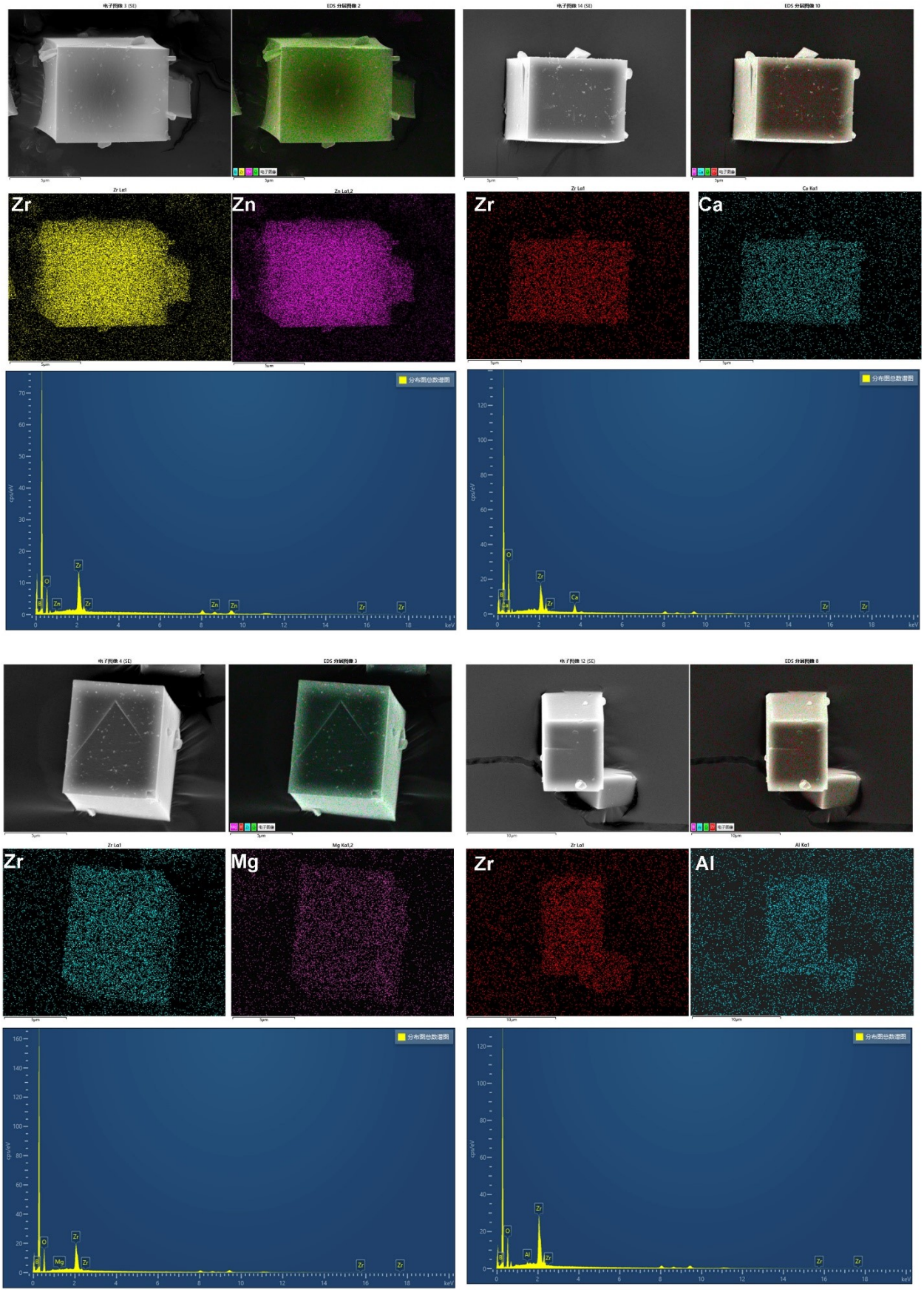

Figure S64. SEM and SEM-EDS mapping of $\mathbf{2}^{\mathbf{Zn}}$, $\mathbf{2}^{\mathbf{Ca}}$, $\mathbf{2}^{\mathbf{Mg}}$, and $\mathbf{2}^{\mathbf{Al}}$.